

MAGNETIC HEATING OF Fe_3O_4 NANOPARTICLES AND MAGNETIC MICELLES FOR A
MAGNETOTHERMALLY-TRIGGERED DRUG DELIVERY SYSTEM FOR CANCER
THERAPY

by

JAMES BRANDON BENNETT

CHRISTOPHER S. BRAZEL, CHAIR

YUPING BAO

DAVID E. NIKLES

A THESIS

Submitted in partial fulfillment of the requirements
for the degree of Master of Science
in the Department of Chemical and Biological Engineering
in the Graduate School of
The University of Alabama

TUSCALOOSA, ALABAMA

2012

Copyright James Brandon Bennett 2012
ALL RIGHTS RESERVED

ABSTRACT

Magnetic nanoparticles, MNPs, combined with stimuli-responsive polymers show potential to enhance the efficacy of cancer therapy in multifunctional nanoscale drug delivery systems. This project investigates the use of iron oxide nanoparticles (magnetite) to generate heat, via an applied magnetic field, to stimulate drug release of doxorubicin from an RGD-peptide targeted thermo-sensitive poly (ethylene glycol)-*b*-poly (caprolactone) micelle. Fe₃O₄ nanoparticles custom synthesized at UA show the ability to heat to temperatures adequate for melting a semi-crystalline poly (caprolactone) micelle core. Investigations into parameters effecting magnetic heating of Fe₃O₄ included studying the effects of magnetic field strength, *H*, and frequency, *f*. The results showed magnetic heating of the MNPs could induce hyperthermic temperatures. Specific absorption rates (SAR) for the MNPs were in the range of previously reported magnetite SARs, and followed the relationship with magnetic field strength predicted by the Rosensweig equation. The internal energy change in magnetic micelles was larger than that observed for MNPs in hexane when heated by an AC magnetic field.

Drug release studies using triamterene- and doxorubicin- loaded micelles show a temperature-dependent acceleration of drug release at temperatures above 42 °C, the melting point of poly (caprolactone), as well as the possibility of magnetic induction hyperthermia-activated release.

DEDICATION

This thesis is dedicated to everyone who helped me and guided me through the trials and tribulations of creating this manuscript—in particular, my family and close friends who stood by me throughout the time taken to complete this work—and my fiancé Whitney for her support.

ACKNOWLEDGMENTS

I am delighted to have this opportunity to thank my colleagues, friends, and faculty members who have helped me throughout this research project. I am most indebted to Chris Brazel, the chairman of this thesis, for sharing his research expertise and wisdom regarding biomaterials, drug release, and magnetic heating. I would also like to thank all of my committee members, David E. Nikles and Yuping Bao for their invaluable input, and support of both this thesis and my academic progress. I would also like to thank Amanda Glover for her support.

CONTENTS

ABSTRACT.....	ii
DEDICATION.....	iii
ACKNOWLEDGMENTS	iv
LIST OF TABLES.....	viii
LIST OF FIGURES	ix
1. INTRODUCTION	1
2. BACKGROUND	2
2.1 Drug delivery systems (DDS) for chemotherapy: controlling and targeting drug delivery	6
2.1.1 Drug delivery system design: materials and controlled release	6
2.1.2 Targeted drug delivery systems	9
2.2 Nanomaterials and magnetic nanoparticles	9
2.3 Magnetic heating and magnetic fluid hyperthermia.....	12
2.5 MNPs in multi-purpose stimuli-responsive nanosystems	18
2.6 Applications of multi-functional nanosystems with MNPs and stimuli-responsive polymers.....	19
3. MOTIVATION	20
4. OBJECTIVES	23
5. MATERIALS AND PROCEDURES.....	25
5.1 Materials studied for magnetic heating characterization.....	25

5.1.1	Magnetic nanoparticles and solvents	25
5.1.2	Magnetic micelles: precursors and preparation	26
5.1.2.1	Block copolymer synthesis.....	26
5.1.2.2	Magnetic micelle preparation.....	27
5.2	Magnetic heating experimental method and procedure.....	29
5.3	Materials for drug release studies.....	34
5.3.1	Drug-loaded micelle preparation	39
5.4	Drug release experimental procedure.....	40
6.	RESULTS AND DISCUSSION	45
6.1	Magnetic heating investigation	45
6.1.1	Effect of magnetic field intensity on the magnetic heating of magnetite.....	45
6.1.2	Frequency modulated magnetic heating studies	53
6.1.3	Magnetic heating with non-solenoid coils	55
6.1.4	Magnetic heating of magnetic micelles	58
6.1.5	Comparison of Fe ₃ O ₄ heating in hexane vs. magnetic micelles	58
6.2	Drug release	62
6.2.1	Triamterene release.....	62
6.2.2	Temperature-dependent Dox release	64
6.2.3	Magnetically-activated drug release investigation.....	66
7.	CONCLUSIONS.....	68
8.	RECOMMENDATIONS	70
	REFERENCES	72

APPENDIX77

LIST OF TABLES

2.1	Stimuli-responsive polymers used in drug delivery with their applications.	8
2.2	SAR determinations for magnetite nanoparticles in aqueous solutions	17
5.1	PEG-PCL diblock copolymers degree of polymerization and molecular weights with corresponding polydispersity indices	28
5.2	Dimensions of magnetic induction coils for magnetic heating experiments.....	30
5.3	Experimental design of magnetic heating investigations: lists of voltages and frequencies tested using different coil types for corresponding magnetic samples	33
6.1	Calculated magnetic field strengths for corresponding voltages used in selected magnetic heating experiments using a 4-turn induction coil without using the frequency modulation coil.....	47
6.2	Calculated added energy values for Fe ₃ O ₄ MNPs in hexane and magnetic micelles in PBS pH 7.7 heated by an AC magnetic field with a fixed frequency of 266 kHz at three magnetic field strengths.....	61

LIST OF FIGURES

3.1	Schematic showing the thermo-responsive behavior of a drug- loaded PEG-b-PCL magnetic micelle	22
5.1	Experimental set-up for magnetic heating studies	31
5.2	Chemical structures of (a) triamterene MW=253.26 and (b) doxorubicin MW=543.52	35
5.3	Calibration plot of different concentrations of triamterene in H ₂ O with absorbance data recorded by a UV-Vis spectrophotometer at a wavelength of 365 nm	36
5.4	Calibration plot of different concentrations of doxorubicin-hydrochloride in HEPES/EDTA pH 7.2 with absorbance data recorded by a UV-Vis spectrophotometer at a wavelength of 485 nm	37
5.5	DLS number average size results data for PEG ₅₃ PCL ₄₉ magnetic micelles with a mean size of 78.8 nm with narrow size distribution	38
5.6	Schematic of experimental set-up for temperature dependent Dox release from Dox-loaded micelles and Dox-loaded magnetic micelles	42
6.1	Magnetic heating profiles for 8.4 g/L Fe ₃ O ₄ nanoparticles in hexane using a 4-turn coil at five magnetic field intensities and a frequency of 266kHz	48
6.2	Calculated SAR values for increasing field strengths for heating 8.4 g/L Fe ₃ O ₄ MNPs in a 4-turn coil, at a frequency of 266 kHz	50
6.3	Plot of SAR values obtained from magnetic heating of Fe ₃ O ₄ in a 4-turn coil, at a frequency of 266kHz as a function of H^2	52
6.4	Magnetic heating curves for 8.4 g/L magnetite nanoparticles in hexane for a 6-turn coil at multiple frequencies and magnetic field strengths	54

6.5	Magnetic heating curves for 8.4 g/L magnetite sample in hexane using a Petri dish coil at 400, 500, and 600V and a frequency of 194 kHz	56
6.6	Magnetic heating curves for 8.4 g/L magnetite sample in hexane using a paper clip coil at 600 V and frequencies of 204, 192, and 133 kHz.....	57
6.7	Magnetic heating curves for MNP-loaded PEG ₅₃ PCL ₄₉ micelle sample in hexane using 4-turn coil at a magnetic field strength of 82.7 kA/m and a frequency of 266 kHz	60
6.8	Release of triamterene from PEG ₄₂ PCL ₁₉ micelles subjected to temperature increase from 37 °C to 47 °C after 20 minutes	63
6.9	Doxorubicin release from PEG ₅₃ PCL ₄₉ micelles at 37 °C and 57 °C based on theoretical loading of 19 wt%	65
6.10	Absorbance values of triple replicate trials of drug release from Dox-loaded PEG ₅₃ PCL ₄₉ micelles.....	67
A1.1	Heating curves for 8.4 g/L Fe ₃ O ₄ in hexane using a 6-turn coil at voltage setting of 400, 500, and 600V at a frequency of 265 kHz	79
A1.2	Magnetic heating curves for 8.4 g/L Fe ₃ O ₄ in hexane using a 4-turn coil at a voltage setting of 600V at frequencies of 266, 204, and 137 kHz.....	80
A1.3	Magnetic heating curves for 8.4 g/L Fe ₃ O ₄ in hexane using a Petri dish coil at a voltage setting of 600V at frequencies of 194, 166, and 124 kHz.....	81
A1.4	Magnetic heating curves for magnetic micelles.	82
A1.5	Magnetic heating curves for 98% pure hexane using a 6-turn coil.....	83
A1.6	Magnetic heating curves for 98% pure hexane using a 4-turn coil.....	84
A1.7	Magnetic heating curves for PBS pH 7.7	85

Chapter 1

INTRODUCTION

Cancer persistently remains one of the leading causes of death in the United States and worldwide. Importantly, there has not been same significant improvement in death rates over recent decades as has been seen for other serious health concerns such as heart disease. Advances in cancer therapy usually focus on improving one of three traditional modes of treatment: surgery, radiation, or chemotherapy; or a combination of these modes. Hyperthermia, which uses elevated body temperature to cause cell death in tumors, is another mode of cancer treatment gaining interest especially when combined with other methods. Research efforts often aim to increase effectiveness by focusing treatment onto a tumor site and minimizing any effect on surrounding healthy tissue. In addition to drug discovery for chemotherapy, there is an increasing interest in developing drug delivery systems (DDS) with abilities to target, image, and control or trigger drug release. Biocompatible polymers and advancements in nanotechnology have led to the development of microspheres, nanospheres, liposomes, hydrogels, nanogels, micelles as promising tools for designing effective DDS.

Magnetic nanoparticles (MNPs), specifically biocompatible iron oxide nanoparticles, show the potential for use as a contrast agent for imaging as well as a hyperthermia agent when exposed to an alternating magnetic field. These MNPs can be utilized in hydrogels, liposomes, or other drug delivery systems to achieve multi-functionality including as a trigger for drug release. These ideas gave rise to this research project which involves designing a drug delivery system

with a thermally-sensitive, drug-loaded core heatable by magnetic nanoparticles exposed to an alternating current magnetic field to induce drug release at hyperthermia temperatures. This thesis will focus on determining the effect of certain magnetic field parameters to achieve hyperthermic heating using an external magnetic induction coil. The feasibility of such a triggering mechanism in a biocompatible, targeted drug delivery system would show great potential for an effective way to kill cancer cells through a combination of chemotherapy and hyperthermia, while minimizing the severe side effects of chemotherapy treatment.

Chapter 2

BACKGROUND

Though cancer continues to challenge the medical field, significant advances have been made in recent decades in cancer therapies offering alternatives to or complementing physical surgical tumor removal. In addition to new isotopes, localization techniques and equipment developed to more safely deliver radiation therapy [1], chemotherapy, and now hyperthermia have shown important improvements in cancer therapy effectiveness, patient survival, and patient quality of life.

Chemotherapy originated as a cancer treatment method in the 1940s when U.S. Department of Defense scientists investigating possible therapeutic effects of chemical warfare agents, such as mustard gas, hypothesized that such chemicals shown to all but cease the division of certain somatic cells could be used to fatally suppress division of certain cancerous cells [2]. The first animal studies in the development of nitrogen mustard, led to the explosion of the cancer drug discovery and development industry. The following decades saw the development of taxanes, camptothecins, nitrosoureas, anthracyclines, and epipodophyllotoxins. Each of these chemotherapeutic agents, essentially poisons, are antineoplastic agents that act in different ways to attack cells in the process cell division:

- taxanes, such as paclitaxel, promote microtubule assembly to inhibit mitosis;
- camptothecins inhibit topoisomerase I, an enzyme that assists DNA unwinding and replication;

- nitrosoureas, and other alkylating agents, crosslink DNA to prevent DNA unwinding;
- anthracyclines and epipodophyllotoxins inhibit topoisomerase II, a second enzyme responsible for cutting DNA strands for unwinding and replication [3].

While these chemotherapeutic agents are potent and effective avenues for killing cancerous cells and tissue characterized by their rapid cell division and growth, these drugs come along with severe side effects that can limit the tolerable dose, as these agents also act on other rapidly dividing cells in the body. Common chemotherapy side effects include:

- depressed immune system, including suppressed bone marrow production and white blood cell count,
- nausea,
- diarrhea,
- alopecia (hair loss),
- fatigue, and
- anemia (low red blood cell count).

To limit these side effects pharmaceutical researchers and scientists are challenged to develop ways to target drug delivery and control drug release.

Another technique seeing increased investigation as an option to treat certain cancers, both by itself and in adjunct therapy with other cancer treatment methods, is hyperthermia therapy. Hyperthermia treatments elevate body tissue temperature to ranges slightly higher than normal. Temperatures between 41 and 45 °C can damage and kill cancer cells with minimal injury to normal healthy tissue [4- 6]. This selectivity is largely accredited to cancer cells' lack of normal vasculature to supply oxygen and dissipate heat. In studies investigating the effects of hyperthermia on normal tissue and tumor tissue microenvironment, hyperthermia was shown to

have a dual effect. Mild hyperthermia up to 41 °C was shown to increase blood flow and oxygen levels, while temperatures above 41 °C showed a sharp decrease in blood flow, lower oxygen levels, and lowered pH which leads to acidosis [7]. The increased perfusion effects of mild hyperthermia has led to its use alongside radiation therapy, which is less effective on cancer cells exhibiting hypoxia and low pH, as well as alongside chemotherapy [8, 9]. Hyperthermia has also been shown to have cytotoxic effects that involve denaturing proteins, inducing heat shock protein (HSP) production, inhibiting cell repair mechanisms and angiogenesis, and inducing apoptosis [4, 8, 10, 11].

Prescribed cancer therapy regimens almost always include a combination of multiple modes of treatment because of the positive synergistic effects between treatment methods. The concurrent or sequential combination of chemotherapy and radiation is now the standard of care for cancer therapy [12]. Similar synergistic effects are seen when combining hyperthermia with chemotherapy or radiation therapy. The effects of hyperthermia are believed to sensitize cancer cells to increase the effectiveness of chemotherapy, in addition to radiation therapy. For instance, in a recent phase III clinical trial comparing combined chemotherapy and hyperthermia therapy to chemotherapy alone, patients given the combined therapy saw slower tumor growth rates and overall survival rates compared to chemotherapy alone [13]. A separate randomized trial confirmed radiation treatments with concurrent hyperthermia therapy were 24% more effective than radiation alone [5]. Preliminary clinical trial results for a triple-modality therapy on cervical carcinoma, where patients were treated with the combination of full-dose radiation therapy, chemotherapy, and hyperthermia, show promising 90% complete remission rates [14].

2.1 Drug delivery systems (DDS) for chemotherapy: controlling and targeting drug delivery

Current chemotherapy research largely focuses on increasing therapeutic effectiveness and lowering costs of chemotherapy treatments through the design of drug delivery systems (DDS). Such devices aim to deliver medications intact to specific tumor sites in the body, and to control or trigger drug release. In uncontrolled drug delivery, the drug enters the body either orally or intravenously and drug release follows first order kinetics. The release rate is initially high at the absorption site surface and drops exponentially as it enters the bloodstream [15]. This can quickly drop the concentration below a drug's optimal therapeutic range rendering the drug ineffective, as well as lead to adverse side effects on normal healthy tissue near the absorption site. Drug delivery systems contain a drug in a lipid or polymer structure designed to alter a drug's release profile or target the drug to a tumor site— or both—in order to increase the drug's therapeutic effect and limit possible severe side effects.

2.1.1 Drug delivery system design: materials and controlled release

Early drug delivery systems for chemotherapy introduced in the 1970s were based on polymers formed by lactic acid and achieved zero order release rates—slow constant release—controlled by polymer degradation [16]. Such DDS increase a drug's bioavailability, allowing a higher percentage of the dose to reach the target site through passive targeting. Today, polymeric materials continue to provide the most promising avenues of research due to their ease of processing and ability for researchers to tailor desired chemical and physical properties through molecular synthesis. Some polymers commonly used in DDS design are

- poly (lactic acid) (PLA),
- poly (lactic-co-glycolic acid) (PLGA),

- poly (ethylene glycol) (PEG), and
- poly (vinyl alcohol) (PVA).

Custom-synthesized polymers can be arranged into various structures—including hydrogels, thin-films, microspheres, nanospheres, nanocapsules, micelles, liposomes or dendrimers [17] – to trap and release drug molecules.

Recently, the development of stimuli-sensitive polymeric drug delivery systems show potential to adjust drug release rates in response to physical (temperature, ultrasound, light, electricity), chemical (pH), and biological (biomolecules, enzymes) stimuli triggers [18]. Some representative stimuli-responsive polymers and their applications in drug delivery are summarized in Table 2.1. Such systems could allow for chemotherapy drug release to be remotely controlled by an external trigger or naturally triggered by a tumor's natural microenvironment. For instance, Hussein et al. report ultrasound activated anti-cancer drug release from commercially produced ethylene oxide and propylene oxide based micelles. Their results indicated that no significant DNA damage occurred when human leukemia (HL-60) cells were exposed to 10 µg/ml of doxorubicin in 10 wt % polymer for up to 9 hours of incubation. However, with the application of ultrasound, a rapid and significant increase in DNA damage and cell death was observed [19].

Table 2.1. Stimuli-responsive polymers used in drug delivery with their applications.
[Reproduced from reference 20]

Stimulus	Polymer	Application
Temperature	Poly(<i>N</i> -isopropylacrylamide)	Hydrogel
		Doxorubicin release
Ultrasound	Polyanhydride, polyglycolide, polylactide poly(hydroxyethyl methacrylate- <i>co</i> - <i>N,N'</i> -dimethylaminoethyl methacrylate)	Ultrasound-enhanced biodegradation
		Ultrasound-enhanced drug release rate
Magnetic field	Poly(ethylene- <i>co</i> -vinylacetate)	Prompted BSA release from matrix in magnetic field
Oxidation	PEG- <i>b</i> -poly(propylene sulfide)- <i>b</i> -PEG	Oxidation-sensitive polymer vesicle disintegration
Light	Poly(<i>N,N</i> -dimethylacrylamide- <i>co</i> -4-phenyl-azophenyl acrylate) poly(<i>N,N</i> -dimethyl acrylamide- <i>co</i> -4-phnyl-azophenyl acrylamide)	Photo-sensitive active site-gating of streptavidin
		Photo-sensitive active site-gating of streptavidin
Electricity	Poly(ethylenediamine- <i>co</i> -1,10-bis(chloro-carbonyl)decane) polyethyloxazoline/poly(methacrylate)	Electric-sensitive capsule
		Electrically erodible matrix for insulin delivery
Mechanical stress	Dihydrazide-crosslinked polyguluronate poly(methyl methacrylate)/poly(vinyl alcohol) or /cellulose ether	Pressure-sensitive hydrogel
		Pressure-sensitive adhesive
pH	Poly(acrylic acid)- <i>g</i> -PEG	Oral insulin delivery
	PEG- <i>b</i> -poly(l-histidine)	Doxorubicin release
Enzymes	PEG-peptide linker-doxorubicin; Peptide linker = GFLG.	Doxorubicin release by lysosomal enzyme-mediated peptide degradation
	Thiolate PEG- <i>b</i> -poly(l-lysine)	Doxorubicin release by lysosomal enzyme-mediated peptide degradation
Biomolecules	PEO- <i>b</i> -poly(2-glucosyloxyethyl acrylate)	Glucose-sensitive micelle for insulin delivery
	Thiolate PEG- <i>b</i> -poly(l-lysine)	Glutathione-sensitive micelle for anti-sense DNA delivery
	Poly(RCOOH- <i>co</i> -butyl acrylate- <i>co</i> -pyridyl disulfide acrylate); R= -CH ₃ , -CH ₂ CH ₃ or -CH ₂ CH ₂ CH ₃	Glutathione- and pH-sensitive copolymers for oligodeoxynucleotide delivery

2.1.2 Targeted drug delivery systems

Cancer tissue's characteristic defective and leaky vasculature architecture exhibits a tendency to retain macromolecules, termed the enhanced permeation and retention effect (EPR effect). This vascular permeability may be exploited to selectively deliver drugs in polymeric drug carriers ranging from 10-500 nm in size to tumor tissue through passive targeting. For instance, PEG-b-PLGA micelles have been shown to localize in tumor tissue by the EPR effect [21-23]. However, to further improve chemotherapy effectiveness, drug delivery systems are now being designed to actively target a drug to a tumor site by conjugating targeting ligands to the surface of polymeric nanoparticles, liposomes, micelles. Monoclonal antibodies, folic acid, RGD-peptides and adenovirus vectors have been used in developing targeting mechanisms for chemotherapy DDS [24-27]. Each of the small molecules bind to corresponding receptor sites overly expressed on the surface of cancer cells comparative to normal tissue. For example, Guan al. targeted a doxorubicin DDS to integrin binding sites on H2009 and H1299 cancer cell lines by attaching an RGD-containing tetrameric peptide to the surface [28]. The development of complex drug delivery systems with the ability to both target and control release will have a significant impact on cancer therapy. Such an achievement came through advances polymer science and ability to image at the nanoscale through transmission electron microscopy TEM and scanning electron microscopy SEM which led to the emergence of nanotechnology.

2.2 Nanomaterials and magnetic nanoparticles

Nanotechnology has provided tremendous promise for modern drug delivery. Nanoscale materials currently being investigated for medical applications include polymeric nanospheres, liposomes, and micelles as well as carbon nanotubes, metal oxide nanoparticles and nanoshells. By combining advances in polymer science with unique properties these of newly developed

nanomaterials, sophisticated design of drug delivery systems may significantly improve cancer treatment efficacy or provide new treatment options. As an example of such ingenuity, gold nanoshells have been for use in photo-thermal therapy to treat cancer in mice. The gold nanoshells excited by a near-infrared laser heated tumor tissue to 65 °C leading to cancer cell necrosis and tumor shrinkage [29]. In response to such studies, the National Cancer Institute (NCI) established a new vision for future cancer therapy: multifunctional nanodevices for diagnostic imaging, tumor targeting, triggered drug delivery, and monitoring treatment.

A key to meeting the lofty NCI goal may be the use of magnetic nanoparticles (MNPs), a class of nanoparticles that can be manipulated using a magnetic field. MNPs show ability to achieve each of the desired functions mentioned in the National Cancer Institute's model device [30-33]. MNPs exhibit several properties making them favorable candidates for use in drug delivery systems including:

- controllable sizes much smaller than a cell (comparable to a virus, protein or a gene);
- modifiable surface properties to allow attachment to biomolecules [34], targeting ligands, drugs [35], or fluorescent tags[36]; and
- superparamagnetic response to an external magnetic field (at small sizes).

Advances in MNP synthesis over the last decade allow for the preparation of single crystal nanoparticles of tunable size, shape, and magnetic properties [37-40]. MNPs have been made of pure iron and cobalt metals, alloys with platinum and zinc compositions, cobalt and manganese ferrites, and iron oxides such as magnetite (Fe_3O_4) and maghemite ($\gamma\text{-Fe}_2\text{O}_3$). Magnetite and maghemite nanoparticles have gained the most research interest as iron oxides are currently the only MNP materials deemed safe for use in the human body. Solution chemical synthesis methods include iron chloride co-precipitation, constrained co-precipitation, polyol synthesis,

and thermal decomposition/reduction [41, 42]. Sun et al. reported a facile oxide nanoparticle synthesis method through thermal decomposition of iron (III) acetylacetonate to achieve narrow size distribution with sizes tunable by surfactant ratio [43].

MNPs can be dispersed in either organic or aqueous phases depending on the use of surfactants or ligands. Most as-prepared MNPs have a capping ligand, often a mixture of oleic acid and oleylamine. Carboxylic acid groups bind to the MNP and the hydrocarbon extends into the environment providing a hydrophobic surface. The hydrophobic capping ligand binding is labile and dependent on a dynamic equilibrium between bound ligand and free ligand in solution. This allows for ligand exchange with a hydrophilic ligand such as dopamine, dimercaptosuccinic acid or 11-mercaptopundecanoic acid or to render the MNPs water-soluble if desired.

Several chemical processes are available to tailor surface functionalization and/or coating of MNPs. For use in drug delivery systems, surface coating and/or encapsulation is often necessary to prevent agglomeration; assist in the conjugation of drug, biomolecule, or targeting vector; and to minimize interactions with untargeted cells. To meet these needs several polymers have been investigated including poly (ethylene glycol) [44, 45], dextran [46], and chitosan [47-49]. Copolymers, micelles, and liposomes are also seeing heavy research interest as many systems incorporating such materials aim to develop multifunctional, stimuli-responsive nanodevices for cancer diagnostics and therapeutics.

MNPs' response to a magnetic field provides great potential for diagnostic and therapeutic applications. Iron oxide nanoparticles are superparamagnetic at sizes below 20 nm. A superparamagnetic particle is comprised of single magnetic domain acting as a single large magnetic dipole moment that aligns flips orientation to align itself with an applied magnetic field creating a larger magnetic moment. This special magnetic response makes them promising

candidates for use as MRI contrast agents [50, 51] where Fe_3O_4 nanoparticles have shown to significantly decrease T_2 relaxation rates producing a dark-field MRI contrast image.

While gold nanoparticles have been developed for photo-thermal therapy showing cancer killing potential, MNPs also show potential for therapeutic effects through magnetic induction heating hyperthermia. Photo-thermal therapy using Au nanoshells requires a laser source's ability to penetrate through tissue to excite Au nanoshells at its location at the tumor site. This limits the practicality of treating deep seated tumors. Also, the high temperatures reached in the previously mentioned example of photo-thermal therapy risk damaging healthy tissue, and causing tumor cell necrosis, which itself can harbor side effects. MNPs show potential for use with an external alternating current (AC) magnetic field to induce hyperthermia therapy, which, in contrast, shows the ability to treat deep seated tumors and risk minimal side effects.

2.3 Magnetic heating and magnetic fluid hyperthermia

The development of magnetic fluid hyperthermia (MFH) has led to a resurgent research interest in hyperthermia treatment of cancer. Prior methods used for cancer therapy using whole body hyperthermia via heated blankets and regional treatments aimed at sections of the body, exhibited serious side-effects and were deemed inferior to radiation and chemotherapy techniques. MFH utilizes a fluid of magnetic nanoparticles designed to be heated by an external alternating current magnetic field to heat surrounding tissue to hyperthermia conditions. MNPs generate heat under an applied AC magnetic field due to hysteresis loss, and Néel and Brownian relaxation. The influence of each of these loss processes depends on the magnetic properties and crystal size of the nanoparticle. Large nanoparticles (usually $> 30\text{nm}$) contain multiple magnetic domains each with a separate magnetization direction and exhibit ferromagnetic behavior. When

an AC magnetic field is applied domains with magnetization directions aligning with the field elongate while others contract leading to domain boundary displacements. Increasing and decreasing magnetization curves for ferromagnetic materials do not coincide demonstrating “hysteresis loss” where energy is lost to heat. MNPs used for magnetic fluid hyperthermia or for drug delivery system applications are often small single-domain superparamagnetic particles with minimal hysteresis loss. In this case, the AC magnetic field causes magnetic moments to rotate and overcome an anisotropy energy barrier to flip its magnetic orientation to align with the field. This energy is lost to heat as the particle relaxes back to equilibrium through Néel relaxation. A third mechanism for MNP magnetic induction heating, Brownian relaxation can cause heating in larger ferromagnetic particles or small superparamagnetic particles. In this process, the energy barrier for magnetic reorientation is rotational friction as an entire particle rotates in its environment in response to the AC magnetic field [52].

The effective relaxation time, τ , from the combined effect of Néel and Brownian relaxations for monodisperse particle is found by [53]:

$$\frac{1}{\tau} = \frac{1}{\tau_B} + \frac{1}{\tau_N} \quad (2.1)$$

where τ_B is the Néel relaxation contribution and τ_N is the Brownian relaxation contribution.

When particles are surrounded by or chemically attached to a polymer (as is the case in most drug delivery system applications), Brownian motion is limited. Therefore, the heating will be dominated by Néel relaxation which depends on the anisotropy (K_u) and particle volume (V)

where $\tau_0 = 10^9$ s:

$$\tau = \tau_0 e^{\frac{-K_u V}{kT}} \quad (2.2)$$

The total power generated for superparamagnetic nanoparticles exposed to an AC magnetic field can be determined with Rosensweig's model [53]:

$$P = \pi\mu_0\chi_0H^2f\frac{2\pi f\tau}{1+(2\pi f\tau_0)^2} \quad (2.3)$$

where χ_0 is the magnetic susceptibility of the MNPs, f is the applied frequency of magnetic field, and μ_0 is the magnetic moment, H is the intensity or amplitude of the magnetic field, and τ is the relaxation time. For a fixed frequency, f , and field strength, H , the power generation increases as the magnetic moment increases.

Perhaps the most important parameter for MNP magnetic heating investigations is the specific absorption rate (SAR). SAR calculations normalize the heat generated to the mass of a magnetic nanoparticle. SAR values typically have units of W/g and are determined from heating curves for MNPs under an applied magnetic field, calculated by:

$$SAR = C_p \frac{\Delta T}{\Delta t} \frac{m_s}{m_{np}} \quad (2.4)$$

where C_p is the heat capacity of the sample, $\frac{\Delta T}{\Delta t}$ is the initial slope of the heating curve, m_s is the sample mass and m_{np} is the mass of the MNPs in the sample. As $\frac{\Delta T}{\Delta t}$ is determined by the power described by equation 2.3, the SAR for a given MNP sample can be maximized by elevating the intensity or frequency of the magnetic field. Also tuning to an optimal size during synthesis may also enhance the magnetic susceptibility of a MNP to raise the SAR. The importance of maximizing SAR is seen when considering a significantly small tumor where the surface area ratio and contact with surrounding healthy tissue is large. Ideally, a minimal amount of MNP can be targeted to enter the tumor and provide enough heating to reach therapeutic hyperthermia effects in the tumor without overheating the healthy tissue.

Energy generated by magnetic particles under an AC magnetic field is transferred as heat to the surrounding environment where temperature rise can be monitored. Magnetic heating temperature curves could be used to predict temperature profiles in-vivo through mathematical modeling involving equations like Penne's equation for bioheat transfer [54, 55]. Such models would be an essential tool to determine the required MNP concentration, magnetic field intensity and duration of field pulses needed to achieve appropriate hyperthermia conditions for a hyperthermia treatment.

The frequency of the magnetic field used for MNP induction hyperthermia on patients should be kept low enough to avoid interaction between the electromagnetic field and intracellular ions as higher frequencies may produce eddy currents that could be harmful to body tissue [56]. Based on experiments on volunteers, Brezovich [57] established a limit for the product of the frequency f and H equal to 4.85×10^8 A/m-s for a 0.3 m coil for a person to "withstand treatment for 1 hour without major discomfort".

Clinical trials for MFH have started in Europe, initiated by the research group of Jordan [58-61]. Patients were administered ferrifluids (magnetite nanoparticles coated with dextran in aqueous solution) before entering a prototype magnetic induction chamber (resembling an MRI machine) capable of generating magnetic fields from 0-15 kA/m at a frequency of 100 kHz. During the treatment, temperature is monitored and kept within therapeutic temperature thresholds, to prevent thermal ablation or ineffective heating. The prototype is showing success treating tumors found in several sites in the body, such as prostate cancer and brain tumors [61].

The number of variables that can influence experimental SAR values for a certain MNP composition:

- size;
- magnetic field intensity, H ;

- frequency, f ;
- coating viscosity; and
- dispersion status (ratio of nanoparticle to surfactant or coating)

makes it difficult to determine a characteristic SAR value for a MNP material when comparing work from various research groups contributing to the literature. While certain trends such as SAR dependence on particle size or field intensity [62] can be confirmed, an encompassing study on the influence of all parameters on SAR (under standard conditions yet to be established) for a given material would be beneficial. Still, typical SAR values found in MNPs being developed for hyperthermia and DDS applications can be gathered, as summarized in Table 2.2.

Table 2.2. SAR determinations for magnetite nanoparticles in aqueous solutions

Material	Average Core diameter (nm)	H (kA/m)	f (kHz)	SAR (W/g)	Reference
Fe ₃ O ₄ MNPs	7.5	32.5	80	15.6	[63]
Fe ₃ O ₄ MNPs (commercially produced)	9	12	300	1.25	[64]
Fe ₃ O ₄ MNPs	13	32.5	80	39.4	[63]
Fe ₃ O ₄ MNPs	13.2	11	410	87	[65]
Aminosilane coated-Fe ₃ O ₄ MNPs	13	13	520	146	[66]
Dextran coated- Fe ₃ O ₄ MNPs	18	16	55	57	[62]
Fe ₃ O ₄ MNPs (commercially produced)	25	12	300	2.8	[64]

2.5 MNPs in multi-purpose stimuli-responsive nanosystems

Multifunctional drug delivery systems with MNPs and stimuli-responsive polymers are being developed to use the hyperthermic effects of MNPs to trigger drug release. Hilt and Satarkar incorporated Fe_3O_4 nanoparticles into temperature-sensitive poly (N-isopropylacrylamide) (PNIPAAm) hydrogels for magnetically-triggered drug release [67]. Vitamin B12 and methylene blue were loaded into the hydrogels and used as model drugs. When an AC magnetic field of strength 5.3 kA/m and frequency 297 kHz was applied, heat generated by the MNPs (20-30 nm) caused the PNIPAAm hydrogel to collapse and squeeze out the drug. The group showed a significantly higher deswelling ratio and accelerated drug release when the hydrogels were loaded with MNPs and submitted to AC magnetic induction heating.

Another promising nanosystem developed by the Rinaldi research group, suggests the ability to induce local hyperthermia therapy with an onboard means of non-invasive temperature monitoring [68]. The group coated 12 nm Fe_3O_4 nanoparticles with a thermo-sensitive fluorescent polymer from NIPAAm and a fluorescent modified acrylamide monomer. Through the fluorescence change in the monomer, the temperature of nanodevices microenvironment can be measured by fluorescence at a wavelength of 450 nm. As a magnetic field is applied for hyperthermia therapy, the heat dissipated from the MNPs to the body tissue could be monitored non-invasively for better controlled cancer treatment. The PNIPAAm block of the polymer also causes the nanoparticles to contract or shrink at elevated temperatures similar to the behavior seen in the hydrogels developed by Hilt and Satarkar showing the possibility to load and trigger release of ant-cancer agents.

Recently, Sanson et al. has investigated the formation of a new-hybrid vesicle system used to encapsulate MNPs and doxorubicin chemotherapy drug molecules into a thermo-

sensitive shell [69]. In the formation of the system, hydrophobic doxorubicin and maghemite nanoparticles are simultaneously added to an aqueous solution where poly (trimethylene carbonate)-*b*-poly (L-glutamic acid) (PTMC-*b*-PGA) vesicles self-assemble by nanoprecipitation with a semi-crystalline shell trapping the drug and MNPs. Upon application of an AC magnetic field ($H= 2.12 \text{ kA/m}$, $f=500\text{kHz}$), MNP heating increases the fluidity of PTMC shell to allow doxorubicin to diffuse out. This system showed accelerated release with “gentle” heating induced by the magnetic field as well as MRI imaging potential. A drawback to this approach is that PNIPAAm is a material not yet accepted for use in human trials.

2.6 Applications of multi-functional nanosystems with MNPs and stimuli-responsive polymers

Along the lines of the research mentioned in the previous section, this project seeks to develop a multi-purpose device that can be used to enhance combination chemotherapy with hyperthermia. Using biodegradable thermo-sensitive block copolymers that self-assemble to form micelles, hydrophobic anti-cancer drug doxorubicin and hydrophobic magnetite nanoparticles will be trapped in a semi-crystalline core. While the MNPs have potential as MRI contrast agents by themselves, the PEG-PCL micelles have potential to load more drug for chemotherapy or MNPs for hyperthermia therapy than similarly self-assembling liposomes. The PEG corona prevents the system from attaching to biomolecules in the blood to increase the device's bioavailability. Furthermore, molecular linking techniques can be used to attach an RGD peptide targeting ligand to the terminus of the PEG block to selectively bind to integrin receptor expressing cancer cells.

Chapter 3

MOTIVATION

The overall goal of this project is to develop a novel multi-functional DDS capable of targeting cancer cells, delivering hyperthermia and chemotherapy through magnetothermally-triggered drug release, and offering magnetic resonance imaging contrast. Biocompatible, block copolymers consisting of a semi-crystalline poly (caprolactone), PCL, core and a poly (ethylene glycol), PEG, corona can self-assemble to encapsulate magnetic nanoparticles and a hydrophobic cancer drug, doxorubicin. The semi-crystalline PCL exhibits a melting point at temperatures slightly above body temperature dependent on the length of the PCL block. This melting of PCL crystals when heated provides the mechanism for thermally-activated drug release. By embedding magnetite, Fe_3O_4 , nanoparticles into the PCL core, the micelles can be heated by an external AC magnetic field to induce hyperthermia conditions and trigger the thermally-activated drug release. On the PEG corona block an RGD peptide targeting ligand can be attached through maleimide chemistry providing the ability to target tumor cells expressing integrin binding sites. Figure 3.1 is a schematic of magnetothermally-triggered drug release from the PEG-PCL micelle DDS when exposed to an AC magnetic field.

The project presents an array of challenges to meet the DDS design goals. Most importantly the developed DDS must be able to: self-assemble into micelles of a size less than 200 nm with a transition temperature between 40 – 45 ° C, load an effective amount of drug to

treat the tumor, load an adequate amount of MNPs to effectively heat and melt the PCL core at acceptable magnetic field strengths and frequencies, demonstrate magnetothermally-triggered release in cell culture, and demonstrate targeting and therapy of cancer cells in cell culture or animal studies. Demonstrating these capabilities will instill the potential for the DDS to be used in therapy regimens where cancer cells are locally treated with a powerful chemotherapeutic under hyperthermia conditions, increasing the therapeutic index of the drug while reducing side effects and improving the patient's quality of life during treatment.

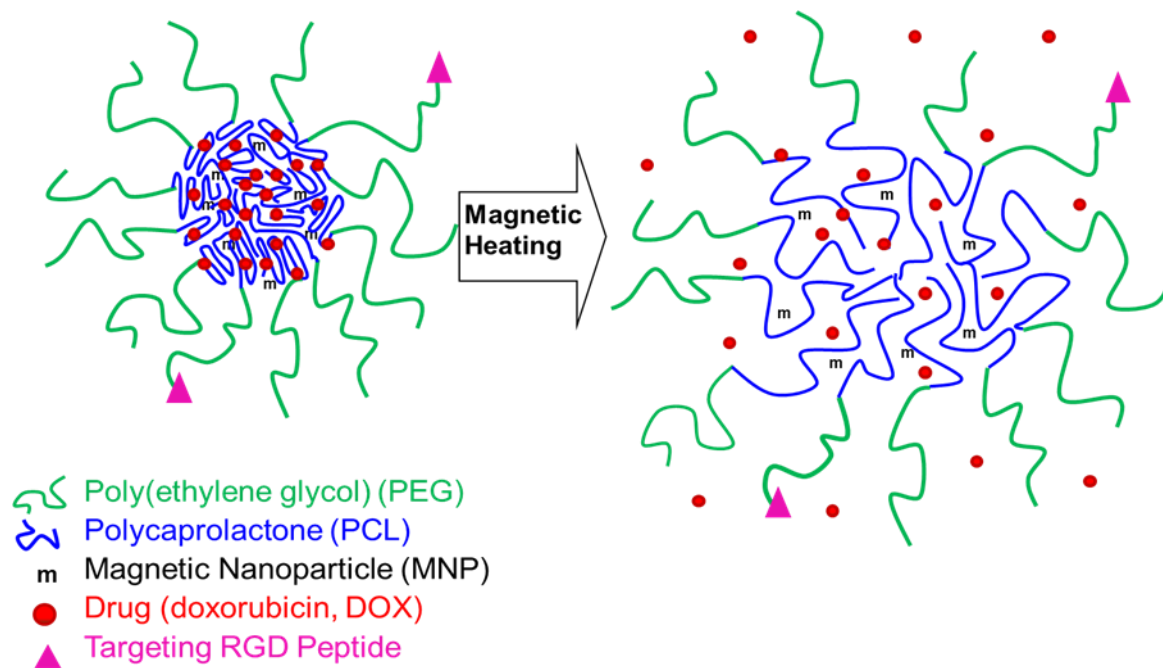


Figure 3.1: Schematic showing the thermo-responsive behavior of a drug- loaded PEG-b-PCL magnetic micelle. Micelle exhibits a PEG corona and a semi-crystalline PCL core that melts when embedded MNPs are exposed to an AC magnetic field heat, triggering drug release.

Chapter 4

OBJECTIVES

For the overall goals of this project to come to fruition, some important characterization and feasibility studies must be made to direct the project's progress. The research in this thesis has focused largely on the magnetic heating capabilities and corresponding design parameters for the proposed DDS. Specific objectives of this thesis project include:

- Characterizing PCL of different molecular weights for melting temperature ranges,
- Preparing drug-loaded and magnetite-loaded PEG-PCL micelles,
- Characterizing of magnetic heating capabilities of the magnetic induction coils in the laboratory including:
 - Effect of magnetic field strength and frequency on magnetic heating,
 - Effect of coil type (coil geometry) on magnetic heating, and
 - Effect of nanoparticle size on magnetic heating.
- Determining the temperature dependence of drug release from doxorubicin loaded micelles, and
- Determining the drug release dependence of magnetothermally-activated drug release by an external magnetic field.

The results of this research will help design future studies to demonstrate the effectiveness of this DDS. This work gives important direction as to which magnetic field strengths and

frequencies will give adequate heating with certain coil types or MNP loading in magnetic micelles, as well as method development for drug release studies to show magnetic field induced drug release.

Chapter 5

MATERIALS AND PROCEDURES

This thesis research is comprised largely of magnetic heating characterization along with drug release experimental design. This chapter describes preparations and characterizations of materials used in these studies, along with a descriptions of the experimental procedures.

5.1 Materials studied for magnetic heating characterization

To characterize the magnetic heating of the MNPs, magnetite particles were investigated in two forms: unencapsulated MNPs in hexane and magnetic micelles with magnetite loaded cores. The magnetite particles were custom synthesized at UA. Magnetic micelles were self-assembled from these magnetite particles and PEG-b-PCL block copolymers also made at UA.

5.1.1 Magnetic nanoparticles and solvents

Magnetite, Fe_3O_4 , nanoparticles were custom synthesized by colleagues in the Nikles lab at UA according to procedures previously reported to give monodisperse nanoparticles of narrow size distribution [43]. Iron (III) acetylacetonate, $\text{Fe}(\text{acac})_3$ and 1,2 hexadecanediol, oleic acid, and oleylamine were added in a 1:5:3:3 molar ratio to a benzyl ether solution and heated to 200 °C for 2 hours then heated to reflux 285 °C for 1 hour under a nitrogen blanket. At room temperature, excess ethanol was added to precipitate a black material that was separated via

centrifugation and redispersed into a hexane/oleic acid solution. The precipitate was washed with additional series of ethanol and hexane washes to yield a dark brown to black dispersion of Fe₃O₄ nanoparticles with an oleic acid coating in hexane. The nanoparticles were dried for storage, requiring redispersion in hexane for TEM imaging and magnetic heating characterization. A 1-mL aliquot of Fe₃O₄ nanoparticles redispersed in hexane was used to study magnetic heating at a concentration of 8.4 g/L.

Deionized (DI) water and n-hexane (98% Fischer Scientific, Pittsburgh, PA) samples were also tested in the magnetic induction coils to determine if any non-specific heating of these solvents may account for any temperature rise.

5.1.2 Magnetic micelles: precursors and preparation

Amphiphilic PEG-b-PCL diblock copolymers were custom synthesized in laboratories at UA to make the thermo-sensitive micelles used in this research. A solvent-evaporation self-assembly technique was used for micelle preparation for its ability to incorporate hydrophobic MNPs and drugs into micelle cores.

5.1.2.1 Block copolymer synthesis

Several formulations of diblock-copolymers with varying PEG:PCL ratios were synthesized by colleagues in the Nikles lab at UA through tin-catalyzed ring opening polymerization of ϵ -caprolactone onto poly (ethylene glycol) [70]. Table 5.1 summarizes the degrees of polymerization and polydispersity indices (PDI) for each of the block copolymers as determined from ¹H NMR spectra of the polymers in CDCl₃ solution obtained on a Bruker Advance 360 Digital NMR (Bruker, Billerica, MA). Molecular weights and PDI were also

determined using a Bruker Ultraflex time-of-flight (TOF) Matrix-assisted laser desorption/ionization spectrometer MALDI-TOF (Bruker, Billerica, MA). The PEG₄₂PCL₁₉ and PEG₅₃PCL₄₉ copolymer formulations were chosen for drug-loaded and Fe₃O₄-loaded micelle preparation due to their larger PCL blocks for MNP loading.

5.1.2.2 Magnetic micelle preparation

Magnetic micelles were prepared for magnetic heating characterization by solvent evaporation self-assembly in phosphate buffer solution at pH 7.7. First, 10.8 mg of PEG₅₃PCL₄₉ diblock copolymer and 4.2 mg of dried Fe₃O₄ nanoparticles were dissolved in 2 mL of filtered tetrahydrofuran THF. The solution was then added dropwise to 25 mL phosphate buffer solution under sonication for vigorous mixing. The solution was then allowed to sit overnight to allow the THF to evaporate. The resulting magnetic micelle solution had a theoretical loading value of 28 % wt Fe₃O₄ per total micelle mass. The solution was then filtered through a 0.45 μm syringe filter to remove any polymer or MNP agglomerations before magnetic heating investigations.

Table 5.1. PEG-PCL diblock copolymers degree of polymerization and molecular weights (M_n) with corresponding polydispersity indices (PDI).

Block Copolymer Composition	M_n (g/mol) [NMR]	M_n (g/mol) [MALDI]	PDI
PEG ₄₄ PCL ₃	~2,400	~2,400	1.02
PEG ₄₃ PCL ₉	~3,000	~2,500	1.02
PEG ₄₂ PCL ₁₉	~4,000	~3,000	1.04
PEG ₅₃ PCL ₄₉	~8,000	~3,000	1.09

5.2 Magnetic heating experimental method and procedure

The magnetic heating characterization experiments were carried out using a custom built magnetic induction hyperthermia unit as depicted in Figure 5.1. The set-up consists of a high frequency AC current generator power supply (0-5kW, NovaStar 5, Ameritherm, Scottsville, NY) which directs the alternating electric current through a looped circuit. The current passes through 1.25 μF capacitors as it enters and exits one of four interchangeable magnetic induction coils of different geometries (4-turn, 6-turn, Petri dish, and paper clip) (Induction Atmospheres, Rochester, NY) which create a magnetic field under which a Fe_3O_4 or magnetic micelle sample generates heat. Table 5.2 provides the physical dimensions of each coil type. These induction coils are water jacketed by a chiller unit to limit the copper coils from overheating. Temperature data were collect using a FLIR ThermaCAM[®] SC2000 (FLIR, North Billerica, MA) infrared camera mounted above the open sample container monitoring the surface temperature of the sample. To adjust the resonance frequency for a certain coil set-up, a frequency modulation coil was placed between the capacitor station and the induction coils to increase the impedance and lower the resonant frequency. A copper bar was also optionally removed from the frequency modulation coils to increase the impedance further and lower the resonant frequency further, to provide a total of three testable frequencies per coil geometry. The initial temperature of each magnetic heating run was kept at 37 °C using a water jacket around the sample in the form of a water filled 1-inch diameter Tygon[®] tube extended from a heated water bath.

Table 5.2 Dimensions of magnetic induction coils for magnetic heating experiments.

Coil Type	Number of turns	Total height (cm)	Inside diameter (cm)	Outer diameter (cm)	Turn spacing (cm)	Spacing note
4-turn	4	4.4	1.85	2.9	0.3	equidistant
6-turn	6	5.4	1.8	2.85	0.1	equidistant
petri-dish	4	5.5	3.8	5	0.2 ^a , 2.0 ^b	non-equidistant
frequency modulation	6	7.1	3.7	5.2	0.6	equidistant
paper clip	2	Short axis length (cm)	Long axis length (cm)		0.25	
		4.2	7.1			

^a spacing between first and second turn, and third and fourth turn pairs

^b spacing between second and third turn

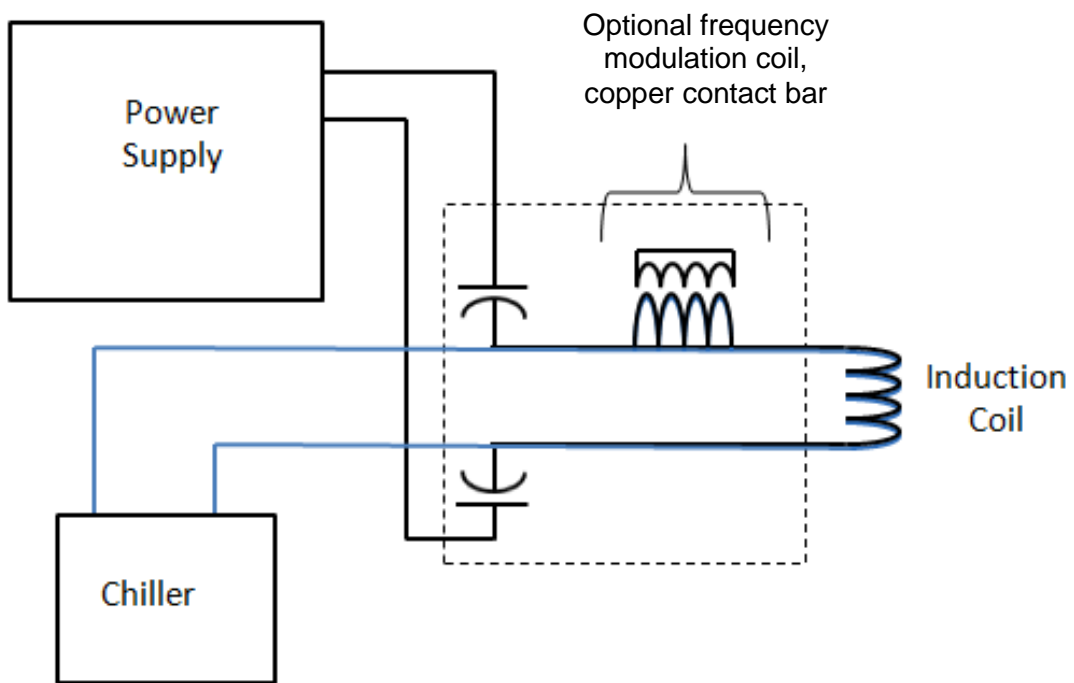


Figure 5.1 Experimental set-up for magnetic heating studies.

For each magnetic heating experiment, the voltage was set by securing circuit contacts within the power supply for voltage setting of 300, 400, 500 or 600 V; and the power supply door was closed and securely refastened. The voltage could be further tuned using a dial on the front of the power supply. The chiller unit was powered on and allowed to reach a temperature of 18 °C before powering up the power supply unit. 0.5 mL of the sample (Fe_3O_4 , magnetic micelle solution, or solvent) was loaded into a plastic Eppendorf tube and placed into the water-jacketing tube positioned so the sample was in the center of the projected magnetic field for the 4-turn or 6-turn coil or where a Petri dish would lay for the Petri dish coil or at an axial distance of either 1 cm or 5cm from the center of the paper clip coil. The infrared camera was turned on and set points positioned and focused such that temperatures of the sample surface, coil surface, and ambient surfaces could be measured. The initial temperature was noted. Then, the magnetic field was activated at the power supply and temperatures were recorded by hand at short 5 second intervals for the first 30 seconds and at 15 second intervals thereafter, for an overall run time of 10 minutes. The resonant frequency readout was displayed on the screen of the power supply and was recorded. Heating experiments were done in three replicates for statistical purposes.

The magnetic heating experiments in this work aimed to investigate the effects of magnetic field strength and frequency on the heating ability of our synthesized nanoparticles and magnetic micelles to for each coil type. Table 5.3 shows the experimental design to investigate magnetic heating to cover this range of experimental variables.

5.3 Experimental design of magnetic heating investigations: lists of voltages and frequencies tested using different coil types for corresponding magnetic samples.

Sample	Investigated Experimental Parameters							
	4-turn		6-turn		Petri dish		Paper clip	
	Voltage (V)	<i>f</i> (kHz)	Voltage (V)	<i>f</i> (kHz)	Voltage (V)	<i>f</i> (kHz)	Voltage (V)	<i>f</i> (kHz)
Fe ₃ O ₄ NPs 8.4 g/L in hexane*	180							
	255							
	300	266	400	265	400	194		237
	360	204	500	185	500	166	600	192
	400	137	600	131	600	124		133
	500							
	600							
Magnetic micelles Fe ₃ O ₄ NPs/ PEG53PCL49 in phosphate buffer solution pH 7.7 0.168 g/L**	400							
	500	266						
	600							

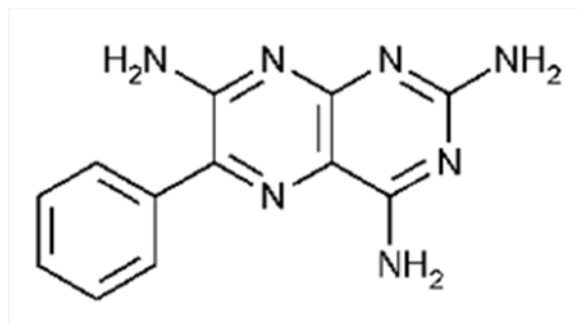
*experimental concentration based on drying in vacuum oven & gravimetric measurements

**theoretical Fe₃O₄ concentration based on synthesis procedure.

5.3 Materials for drug release studies

The solvent-evaporation method was also used to prepare drug-loaded micelles for drug release studies. The initial study used triamterene (Aldrich, St. Louis, MO) as a model drug encapsulated into the micelle core in place of expensive doxorubicin (Dox) for a temperature modulated release experiment. Dox-loaded micelles and Dox-loaded magnetic micelles were then prepared for temperature-dependent and magnetothermal-activation-dependent drug release investigations. Figure 5.2 shows the structures of the triamterene and doxorubicin; both are small, highly hydrophobic molecules. Micelles were prepared in ultrapure water for the initial experiment while a hydroxyethyl piperazineethanesulfonic acid /ethylenediaminetetraacetic acid (HEPES/EDTA) buffer solution pH 7.2 was used for subsequent micelle preparations allowing such solutions to be used in cell-binding and cell death studies. UV-Vis calibration data and magnetic nanoparticle size distribution via dynamic light scattering DLS using a Zetasizer Nano ZS (Malvern Instruments, Malvern, UK) are shown in Figures 5.3 -5.

(a)



(b)

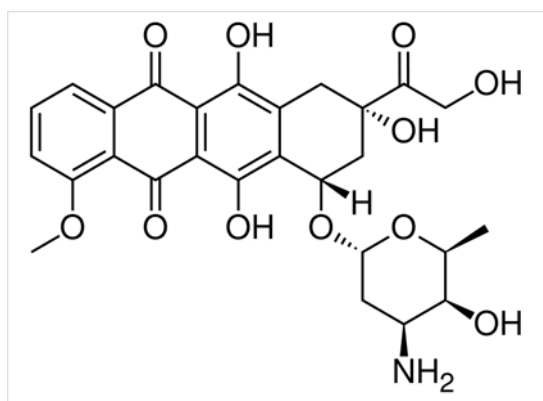


Figure 5.2. Chemical structures of (a) triamterene MW=253.26 and (b) doxorubicin MW=543.52.

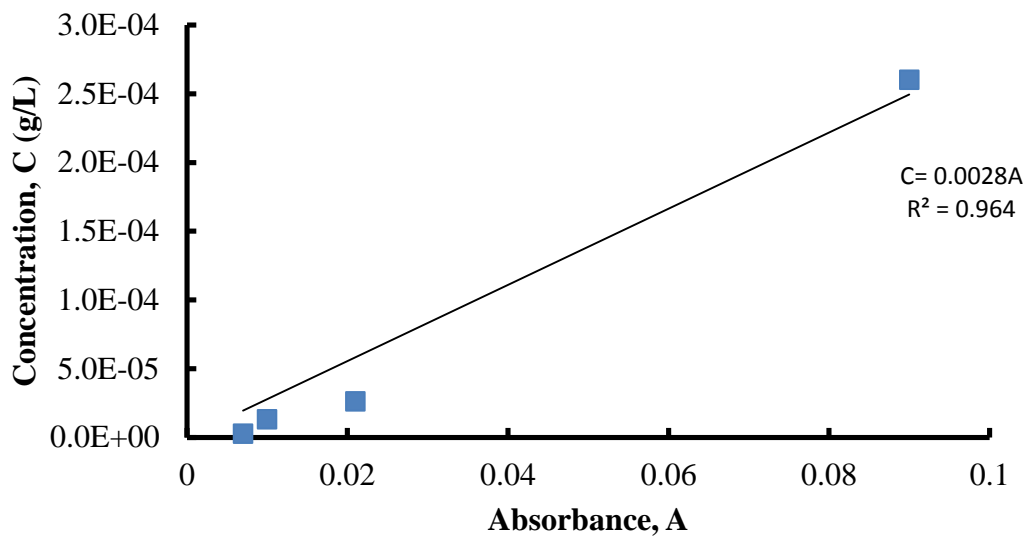


Figure 5.3. Calibration plot of different concentrations of triamterene in H₂O with absorbance data recorded by a UV-Vis spectrophotometer at a wavelength of 365 nm.

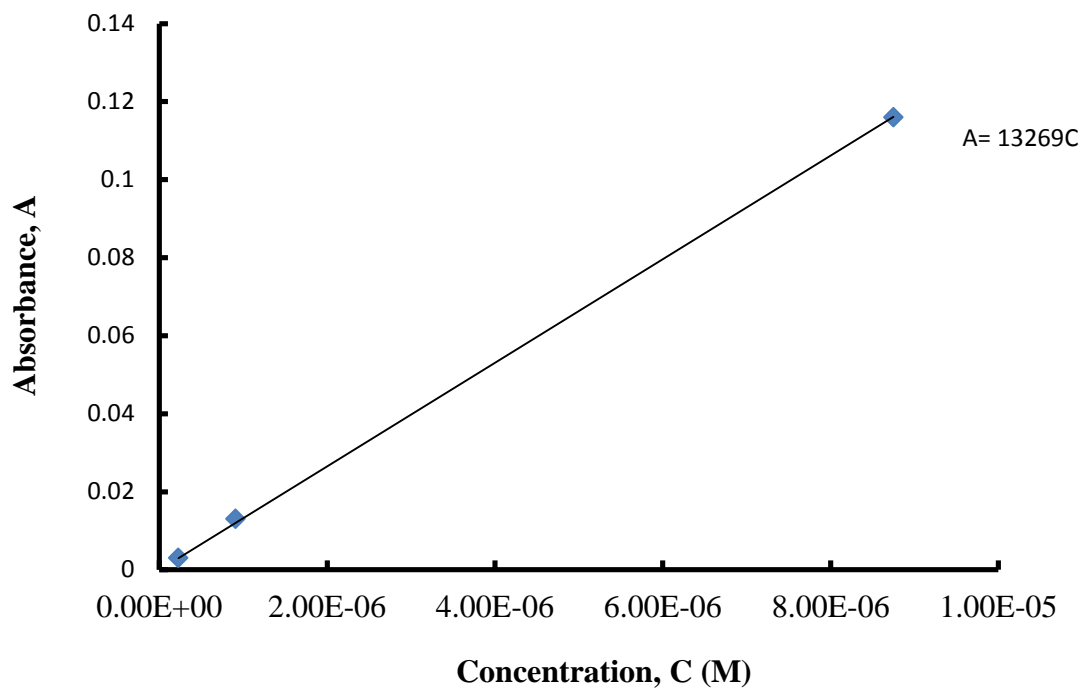


Figure 5.4 Calibration plot for different concentrations of doxorubicin-hydrochloride in HEPES/EDTA pH 7.2 with absorbance data recorded by a UV-Vis spectrophotometer at a wavelength of 485 nm.

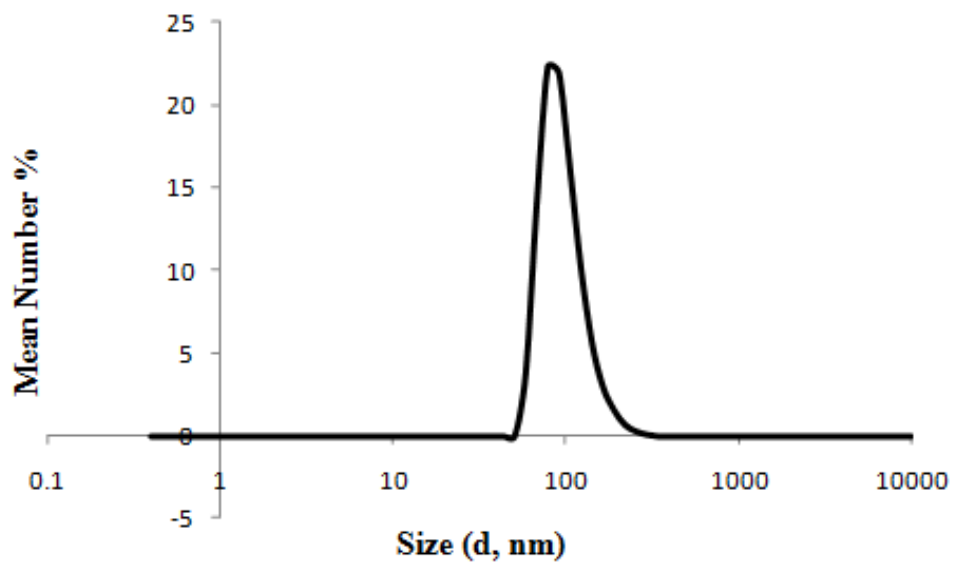


Figure 5.5. DLS number average size results data for PEG₅₃PCL₄₉ magnetic micelles with a mean size of 78.8 nm with narrow size distribution.

5.3.1 Drug-loaded micelle preparation

Triamterene- and doxorubicin-loaded micelles and doxorubicin-loaded magnetic micelles were prepared following procedures similar to those used for the magnetic micelle preparation mentioned earlier in this chapter. For the triamterene experiment, 10.1 mg of PEG₄₂PCL₁₉ diblock copolymer and 1 mg of triamterene were dissolved in 2 mL of filtered tetrahydrofuran THF. The solution was then added dropwise to 25 mL ultrapure water under sonication for vigorous mixing. The solution was then allowed to equilibrate overnight uncapped to allow THF to evaporate. Any residual THF was removed through rotary evaporation as the solution was concentrated to a total volume of 10 mL. The resulting solution was filtered through a 0.45 µm syringe filter to remove any aggregates and ultrafiltered through a 50 kDa molecular weight cut off (MWCO) centrifugal filter device to remove free triamterene. A 1-mL aliquot was used for the drug release experiment.

Dox-HCl (Aldrich, St. Louis, MO) was purchased for the preparation of Dox-loaded micelles and Dox-loaded magnetic micelles. An additional deprotonation step using excess triethylamine (Aldrich, St. Louis, MO) was required to achieve the hydrophobic doxorubicin structure needed for micelle drug loading. The Dox-loaded micelles used in a temperature dependent drug release experiments were prepared by adding 2.6 mg Dox-HCl and 7.3 mg triethyleamine to a 1 mL THF solution with stirring. 0.3 mL DMSO was added to completely solubilize the doxorubicin to give a clear red solution. 10.3 mg PEG₅₃PCL₄₉ dissolved in 1 mL THF was added and the Dox/TEA/copolymer/THF/DMSO solution was added dropwise to 6 mL of HEPES/EDTA buffer solution (50mM/10mM, pH 7.24) with sonication. These micelles were dialyzed against a 50 kDa MWCO membrane in HEPES/EDTA (50mM/10mM, pH 7.24) at 4 °C

for 24 hours. 1-mL aliquots of this Dox-loaded micelle solution were used for temperature-dependent drug release experiments.

Dox-loaded magnetic micelles were prepared in a similar fashion, In this case, 0.5 mL DMSO was added to 1.4 mg Dox-HCl and 7.3 mg triethylamine (TEA) in 2 mL of THF with magnetic stirring to completely solubilize the doxorubicin. The Dox/TEA/THF/DMSO solution was added to a solution of 10.0 mg PEG₅₃PCL₄₉ in 0.4 mL THF and that solution was added to a solution of 3.9 g Fe₃O₄ nanoparticles dissolved in 0.8 mL THF. The resulting Dox/TEA/copolymer/Fe₃O₄/THF/DMSO solution was added dropwise to 10 mL of HEPES/EDTA buffer solution (50mM/10mM, pH 7.24) with sonication. The micelle solution was then dialyzed against a 50 kDa MWCO membrane in HEPES/EDTA (50mM/10mM, pH 7.24) at 4 °C for 24 hours. The solution was diluted to total volume of 10 mL and filtered through a 0.45 µm syringe filter. 1 mL aliquots of the solution were used for magnetothermal-activation drug release experiments.

5.4 Drug release experimental procedure

Temperature-dependent drug release and pulsed magnetothermally-activated drug release were investigated using a preassembled dialysis device. A Float-A-Lyzer G2 (Spectrum Laboratories, Rancho Dominguez, CA) 50kDa MWCO cellulose ester membrane dialysis device with a 1 mL sample capacity was used for release experiments, as the micelles could be retained inside the Float-A-Lyzer while free (released) drug diffused across into the dialysate which could be measured by UV-Vis. The device caps the membrane with a plastic housing with a removable screw top lid and a Styrofoam ring to assist in floatation. Isotemp 210 and Precision Shaking Bath model 50 (Thermo-Fisher Scientific, Waltham, MA) water baths were used to keep the

temperature constant. A Shimadzu UV2401 Spectrophotometer (Shimadzu, Columbia, MD) was used to monitor the absorbance of the dialysate samples.

Triamterene-loaded micelles were used in a temperature modulated drug release experiment. A Float-A-Lyzer device was pre-soaked with DI water for 30 minutes, rinsed, and emptied before a 1-mL sample of the triamterene-loaded micelle solution was placed into the device. The dialysis device floated in a 100 mL dialysate of DI water at a temperature held constant at 37 °C. Dialysate samples (1 mL) were taken and replaced with fresh DI water every four minutes. After 20 minutes, the dialysis device was moved to a new 100 mL dialysate at constant temperature of 47 °C to mimic magnetic heating above the melting point of PCL. Triamterene concentrations in the dialysate were monitored by UV-Vis spectrophotometry at a wavelength of 365 nm.

Dox-loaded micelles were investigated in isothermal drug release studies at 37 and 57 °C. Again, a pre-soaked and rinsed Float-A-Lyzer was filled with 1 mL of a Dox-loaded micelle solution. The device was placed in a smaller 12 mL HEPES/EDTA dialysate release medium to increase sample UV-Vis absorbance. The temperature was held constant at 37 °C for 48 hours for three trials and at 57 °C for 48 hours for three trials. 1 mL samples were taken and replaced with 1 mL of fresh HEPES/EDTA buffer solution (50mM/10mM, pH 7.24) every 15 minutes for the first hour, then every 30 minutes for the next three hours, then every hour for the next 5 hours. Samples were then taken and replaced with buffer every 2 to 3 hours for a total release duration of 48 hours. The doxorubicin concentration in the dialysate samples was monitored by UV-Vis spectrophotometry at a wavelength of 485 nm. The experimental setup for temperature dependent Dox release is shown in Figure 5.6.

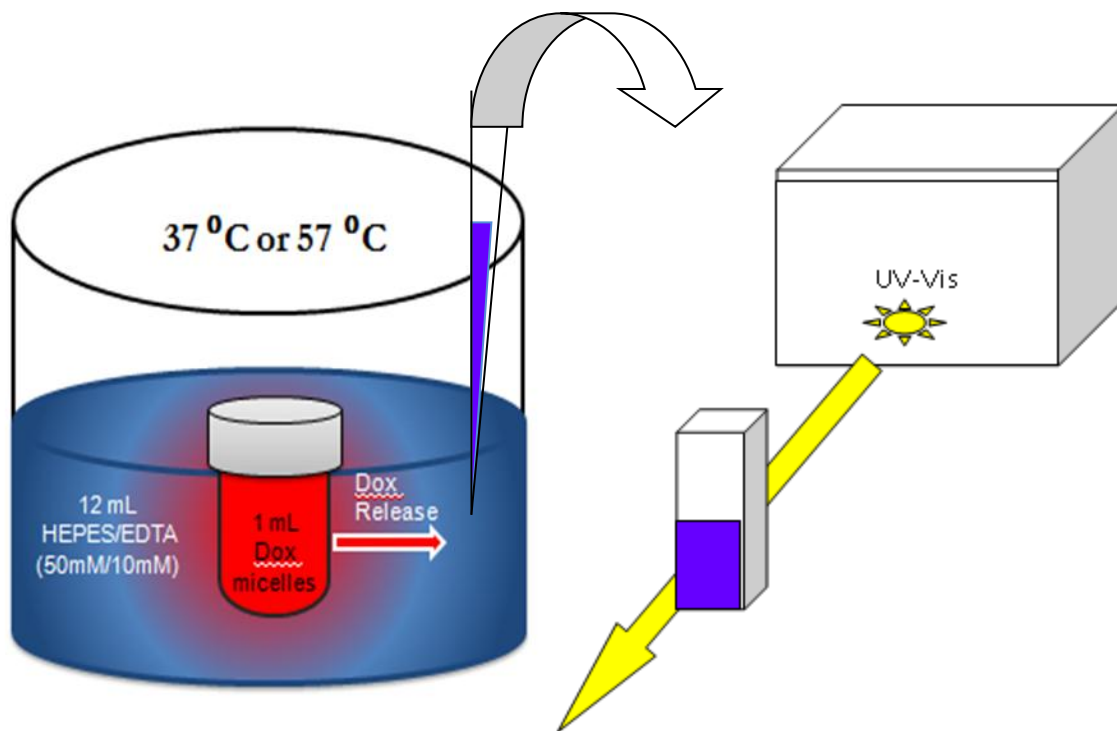


Figure 5.6. Schematic of experimental set-up for temperature dependent Dox release from Dox-loaded micelles and Dox-loaded magnetic micelles. Samples taken from the dialysate release medium are transferred to a quartz cuvette for UV-Vis analysis.

Dox-loaded magnetic micelles were used to investigate magnetothermally-activated drug release. Since the dialysis device and release medium system cannot easily fit into the induction coils, this study utilized non-release periods where the micelle solution was removed from the dialysis device and placed in an Eppendorf tube for either a pulse of magnetic heating or for an isothermal non-release period in an incubating oven for a control. A pre-soaked and rinsed Float-A-Lyzer was filled with 1 mL of Dox-loaded magnetic micelle solution and placed into a 12 mL release medium of HEPES/EDTA buffer solution (50mM/10mM, pH 7.24) in a shaker bath holding a constant temperature of 37 °C. After 30 minutes, a 1 mL sample of the dialysate was taken and replaced with 1 mL of fresh buffer solution and the Dox-loaded magnetic micelle solution was removed from the Float-A-Lyzer and placed into an Eppendorf tube for the non-release period. For three trials, the sample was placed in an 37 °C incubating oven during the non-release period. For another three trials, the sample was placed into the magnetic heating induction coils set up as described in section 5.2 and exposed to a magnetic field at a strength of 74.2 kA/m and a frequency of 266 kHz for 30 minutes. The sample was then placed back into the Float-A-Lyzer in the same 12 mL release medium from which it was removed. The same procedures were repeated for another 30 minute release period, followed by a 30 minute non-release period and a final 30 minute release period. The doxorubicin concentration in the dialysate samples was monitored by UV-Vis spectrophotometry at a wavelength of 485 nm.

A different method of detecting drug release was used for the magnetically-triggered drug release experiment. After extremely low UV-Vis absorbance values obtained for dialysate samples taken at the time points mentioned above were deemed unusable in data analysis, samples from the Dox-loaded magnetic micelle solution inside the Float-A-Lyzer device were taken. UV-Vis absorbance values of these samples were much higher and could be used

comparatively to determine if Dox-loaded magnetic micelles exposed to magnetic field pulses caused showed increased drug release by lowered UV-Vis absorbance.

Chapter 6

RESULTS & DISCUSSION

6.1 Magnetic heating investigation

Magnetic induction heating experiments on magnetite and magnetic micelle samples prepared as described in the previous chapter.

6.1.1 Effect of magnetic field intensity on the magnetic heating of magnetite

Magnetite nanoparticles synthesized by thermal decomposition resulted in black nanoparticles coated in oleic acid. The particles were easily dispersible in hexane to achieve an 8.4 g/L solution of Fe₃O₄ nanoparticles. The concentration was determined by drying out a known volume of the solution in a vacuum oven and weighing the resulting dry nanoparticles with any attached surfactants. This MNP solution was used to investigate the effect of magnetic field intensity, H , on magnetic heating. Using a 4-turn coil, with a resonant frequency of 266 kHz, the only parameter changed was the voltage, modulated by contact points on the circuit board of the power supply, and also by a tunable dial on the front of the power supply. Five relatively high voltages of 180, 255, 300, 360, 400 V were used to heat 0.5 mL of the Fe₃O₄ solution.

An estimation of the magnetic field strength, H , for each experiment was calculated using the following equation:

$$H = \mu_0 IN \quad (6.1)$$

where μ_0 is the permeability constant equal to $4\pi 10^{-7} \text{ N s}^2/\text{C}^2$, I is the current, in amperes, and N is the number of turns per length of coil. The current, I , is calculated by dividing the total voltage, manually set on the power supply, by the impedance, X_c , which can be found by the following equation:

$$X_c = \frac{1}{2\pi f C} \quad (6.2)$$

where f is the resonant frequency, in Hz, reported by magnetic induction unit when powered on, and C is the capacitance which is kept at $1.25 \times 10^{-6} \text{ F}$ by capacitors as constant installations in the experimental set-up depicted in Figure 5.1. The field strengths at each voltage in this experiment are shown in Table 6.1.

Figure 6.1 shows magnetic heating curves for each triple replicate experiment at the different magnetic field strengths using the 4-turn coil at a fixed frequency of 266 kHz. As expected, with increased magnetic field strength came more efficient heating and higher maximum temperatures. Each of the heating curves reached a steady state temperature within two minutes and the experimental runs ended at five minutes.

Table 6.1. Calculated magnetic field strengths for corresponding voltages used in selected magnetic heating experiments using a 4-turn induction coil without the frequency modulation coil.

Voltage Setting (V)	Frequency (f) (kHz)	Magnetic Field Strength (kA/m)
180	266	33.4
255	266	47.3
300	266	55.7
360	266	66.8
400	266	74.3

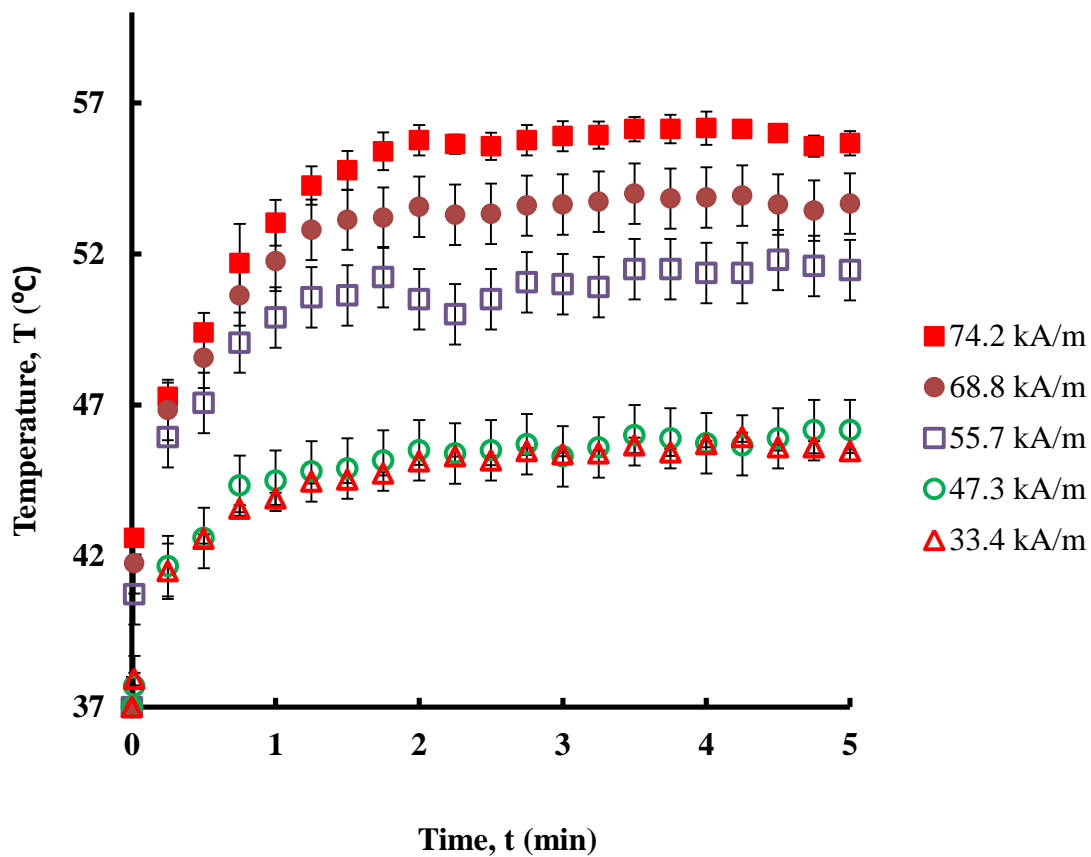


Figure 6.1 Magnetic heating profiles for 8.4 g/L Fe_3O_4 nanoparticles in hexane using a 4-turn coil at five magnetic field intensities and a frequency of 266kHz. Error bars represent the standard deviation for replicate trials, n=3.

Specific absorption rates, SAR, were calculated according to the equation:

$$SAR = C_p \frac{\Delta T}{\Delta t} \frac{m_s}{m_{np}} \quad (2.4)$$

where $\frac{\Delta T}{\Delta t}$ is the initial slope of the magnetic heating curve and the mass of the sample m_s is the combined mass of hexane, 0.5g, and the magnetite nanoparticle mass, m_{np} , 8.4 mg. The heat capacity for the sample, C_p , was determined through a weighted average of hexane and Fe₃O₄ heat capacity values of 180.1 and 194.9 J/mol-K respectively [71].

To determine the initial slope used for $\frac{\Delta T}{\Delta t}$ in the above equation, temperature data representing 66.7% of the maximum temperature change were used to plot θ as a function of time in a curve fit evaluated at $t=0$, where θ is the normalized temperature difference defined as $\frac{T-T_\infty}{T_0-T_\infty}$. T_∞ represents the maximum temperature and T_0 represents the initial temperature. Integrating and evaluating for $\left. \frac{d\theta}{dt} \right|_{t=0}$ gives a slope used for $\frac{\Delta T}{\Delta t}$ in SAR calculations. Figure 6.2 shows SAR values for each of the magnetic field strengths. SAR increases as the magnetic field strength increases. The SAR values for these custom-synthesized Fe₃O₄ nanoparticles range from 35.7 to 110.8 W/g which compare favorably to previously reported SARs mentioned in section 2.4 shown in Table 2.2.

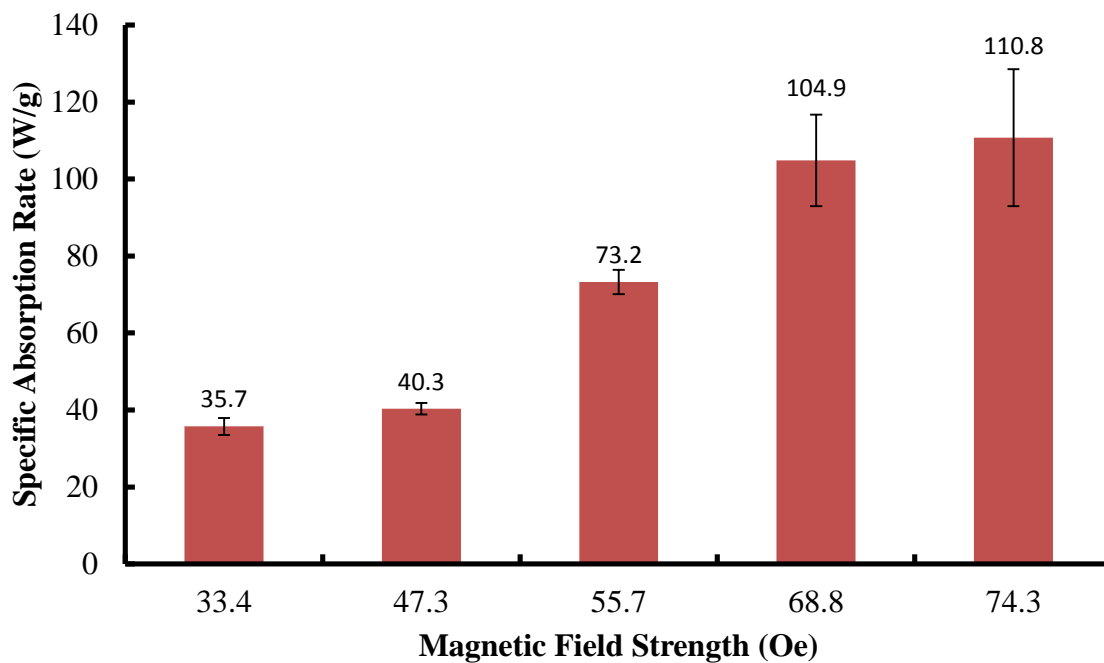


Figure 6.2. Calculated SAR values for increasing field strengths for heating 8.4 g/L Fe_3O_4 MNPs in a 4-turn coil, at a frequency of 266 kHz. Error bars represent standard deviation for replicate trials, $n=3$.

According to the Rosensweig equation for a given particle composition, where magnetic properties will stay constant, the SAR should show a linear relationship with the square of the magnetic field intensity, H^2 ,

$$P = \pi\mu_0\chi_0H^2f \frac{2\pi f\tau}{1+(2\pi f\tau)^2} \quad (2.3)$$

The results achieved in this study were compared with those predicted by the Rosensweig relationship (Figure 6.3). The SAR values are shown as a function of H^2 for the magnetite particles in this experiment. While a linear fit is achieved as predicted by equation 2.3 there is considerable deviation from the fit especially at lower field strengths.

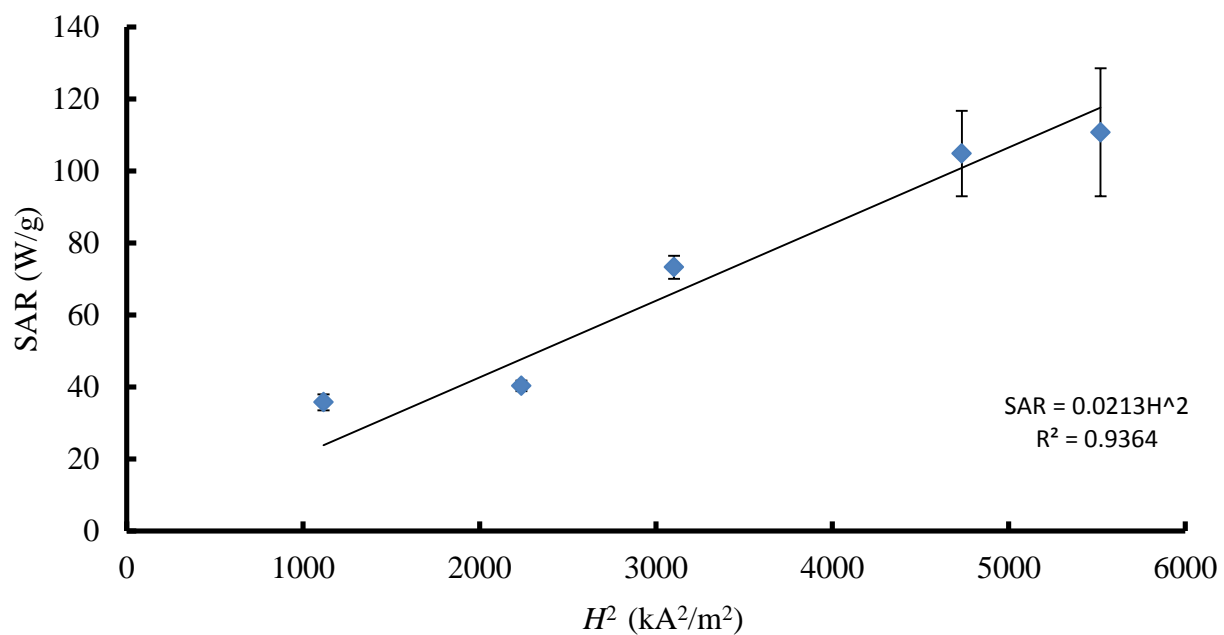


Figure 6.3. Plot of SAR values obtained from magnetic heating of Fe₃O₄ in a 4-turn coil, at a frequency of 266kHz as a function of H^2 . Error bars represent standard deviation for replicate trials, n=3.

6.1.2 Frequency modulated magnetic heating studies

An 8.4 g/L concentrated solution of magnetite particles in hexane were used in a frequency modulated study of magnetic heating with a 6-turn coil. The voltage for this study was set to 600V by securing contacts inside the power supply. The frequency was lowered from 265 kHz used in initial runs to 185 kHz by adding a frequency modulation coil with copper contact bar attached to the circuit for triple replicate trials, then further lowered to 131 kHz by removing the copper contact bar for triple replicate trials. Lowering the frequency also lowers the magnetic field in each case. Estimation methods determined the magnetic field strengths to be 92.5 kA/m, 71.1, and 42.7 kA/m respectively. Figure 6.4 shows magnetic heating curves for the succession of lowered frequencies. The lower frequency and magnetic field clearly lead to less effective magnetic heating. This is confirmed by their calculated SAR values of 42.3, 20.2, and 9.2 (W/g) as the frequency and magnetic fields decrease.

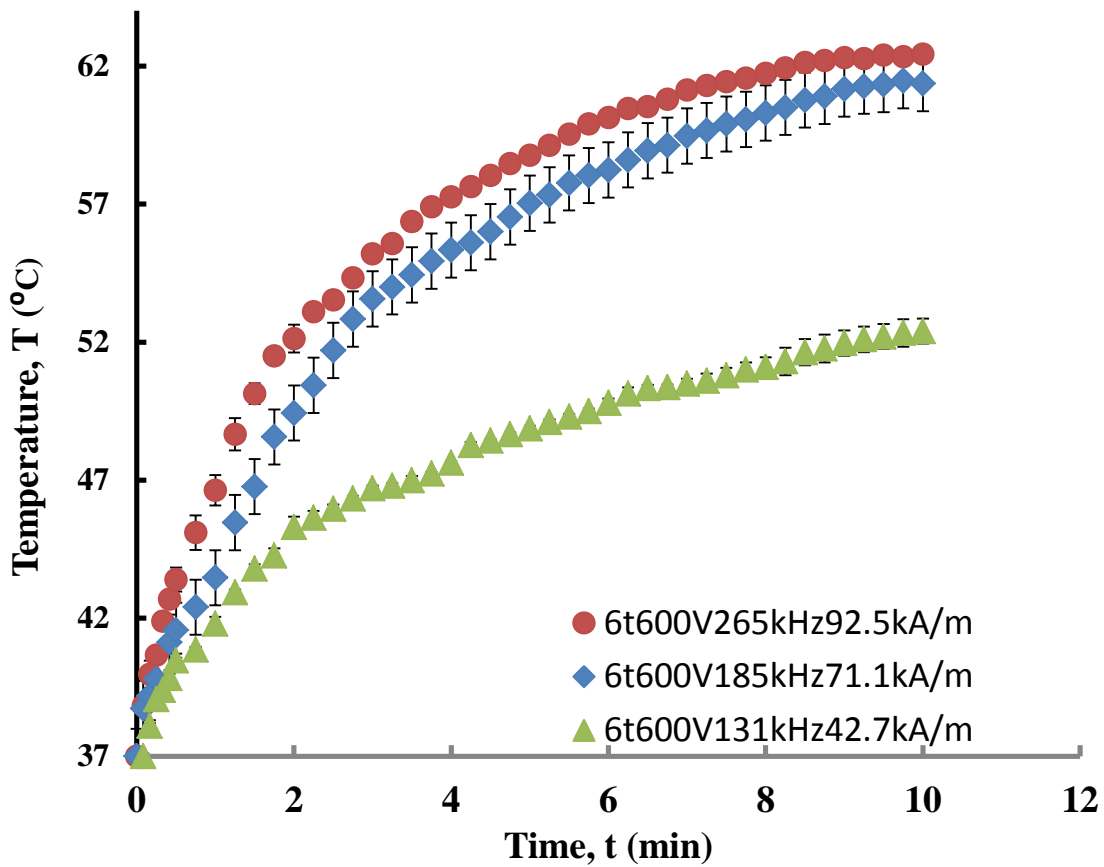


Figure 6.4 Magnetic heating curves for 8.4 g/L magnetite nanoparticles in hexane for a 6-turn coil at multiple frequencies and magnetic field strengths. Error bars represent the standard deviation for $n=3$, in some cases error bars are smaller than the marker.

6.1.3 Magnetic heating with non-solenoid coils

Magnetic heating abilities of the Petri dish and paper clip coils were also investigated using a 0.5 mL aliquot of an 8.4 g/L magnetite sample in hexane. Figures 6.5 and 6.6 show representative magnetic heating curves for the MNP heating experiments using the Petri dish coil and paper clip coil respectively. Figure 6.5 shows data for 400, 500, and 600V settings at 194 kHz on the Petri dish coil, while Figure 6.6 shows data from a paper clip coil experiment at 600 V and frequencies of 204, 192, and 133 kHz. These curves show an irregular shape with a small temperature rise within the first minute followed by continued slow heating. The modified geometry of these coils leads to lower magnetic field intensities and lower magnetic heating when compared to the tighter 4-turn and 6-turn coils. Future plans for animal studies may require a new coil design with a larger diameter solenoid to fit animal specimens. Other temperature data for the Petri dish and paper clip coils, along with data for heating pure hexane and PBS can be found in Figures A1.5-A1.7.

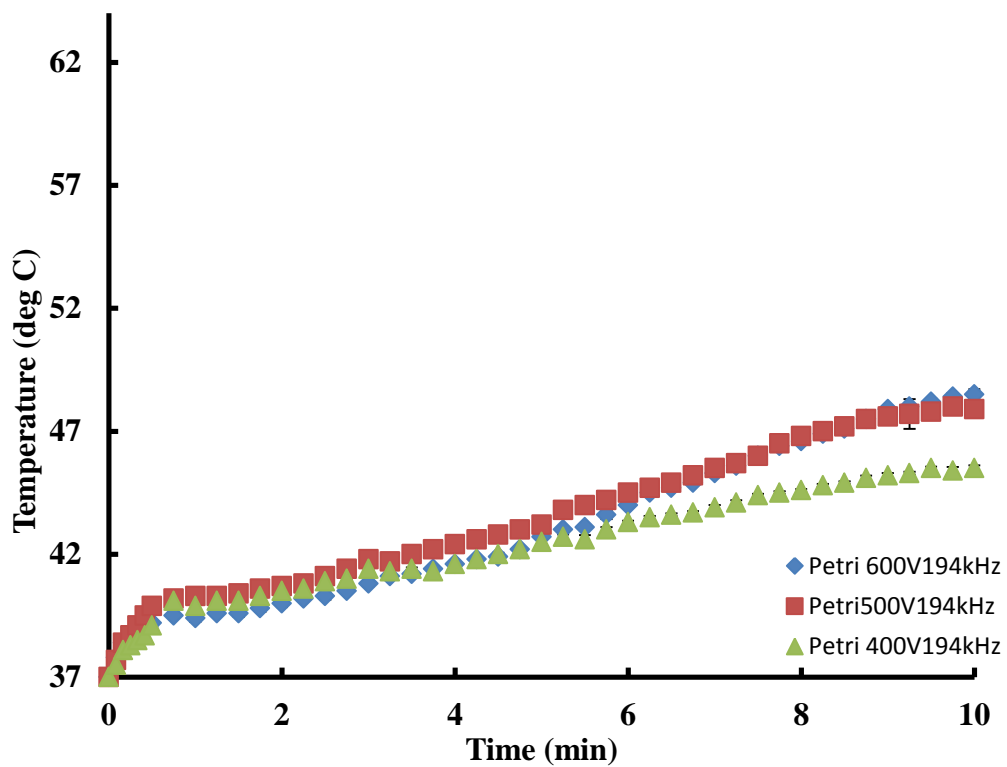


Figure 6.5. Magnetic heating curves for 8.4 g/L magnetite sample in hexane using a Petri dish coil at 400, 500, and 600V and a frequency of 194 kHz. Error bars represent the standard deviation for n=3, in some cases error bars are smaller than the marker.

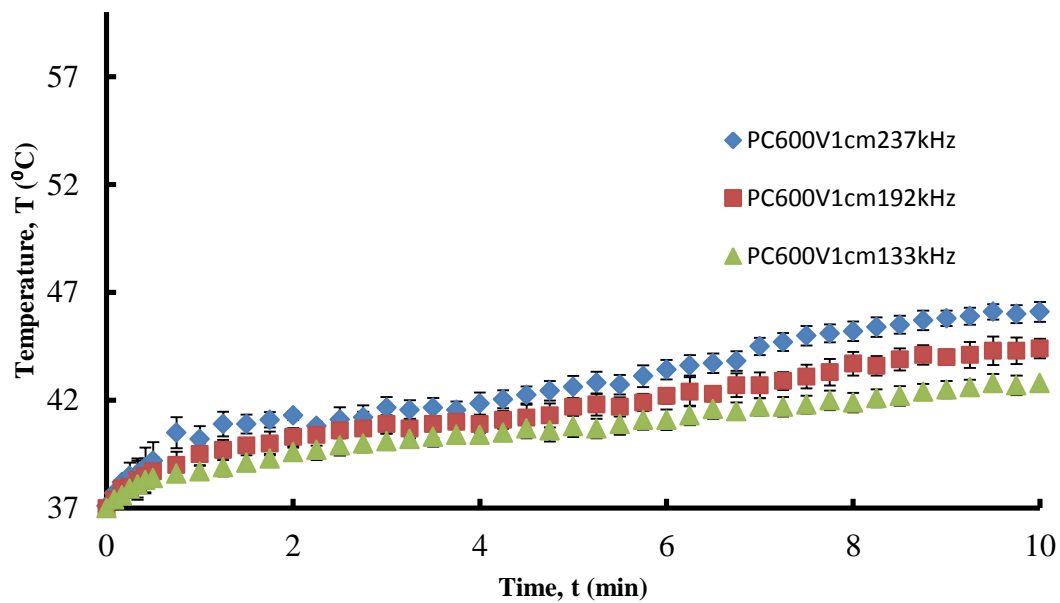


Figure 6.6. Magnetic heating curves for 8.4 g/L magnetite sample in hexane using a paper clip coil at 600 V and frequencies of 204, 192, and 133 kHz. Error bars represent the standard deviation for $n=3$, in some cases error bars are smaller than the marker.

6.1.4 Magnetic heating of magnetic micelles

Magnetic micelles prepared by solvent evaporation techniques to load Fe₃O₄ MNPs into PEG₅₃PCL₄₉ micelles were also investigated for magnetic heating ability. These micelles had a theoretical effective Fe₃O₄ MNP concentration of 0.168 g/L. Figure 6.7 shows a representative magnetic heating curve for the magnetic micelles using a 4-turn coil set to 500V at 266 kHz frequency. The curve does not show a temperature rise until after 60 seconds. This lag time may be explained by MNP heating in micelles first dissipating to the melt PCL core before heating the rest of the micelles/PBS solution of which the surface temperature is reported by an IR camera. After the lag period slow heating is seen requiring 12 minutes to reach 47 °C. Additional heating curves for the magnetic micelles can be found in Figure A1.4.

6.1.5 Comparison of Fe₃O₄ heating in hexane vs. magnetic micelles

To compare the magnetic heating of Fe₃O₄ MNPs loaded in magnetic micelles to the previously discussed results for Fe₃O₄ MNPs in hexane, the total energy added, ΔU , over five minutes was calculated for each system at AC magnetic field strengths of 82.7, 74.2, and 55.7 kA/m and normalized to the mass of Fe₃O₄, $m_{Fe_3O_4}$ (Table 6.2). For the Fe₃O₄ MNPs in hexane and magnetic micelle solution, the internal energy change was calculated according equations 6.3 and 6.4, respectively:

$$\Delta U = m_{soln} C_p \Delta T \quad (6.3)$$

$$\Delta U = m_{soln} C_p \Delta T + m_{PCL} \Delta H_f \quad (6.4)$$

where m_{soln} is the total mass of the heated sample, C_p is the weighted average heat capacity of the sample, ΔT is the average temperature difference obtained over five minutes adjusted to account for any non-specific heating of hexane or PBS (as shown in Figure A1.5-A1.7), m_{PCL} is

the mass of PCL in the micelle sample, and the heat of fusion for PCL, $\Delta H_f = 139.5 \text{ J/g}$ [72].

The calculated internal energy change normalized by the total mass of MNPs in the sample,

$\frac{\Delta U}{m_{Fe_3O_4}}$, for the magnetic micelles were larger than was observed for the Fe_3O_4 MNPs in hexane

by almost an order of magnitude suggesting the confinement of the MNPs in PCL may enhance magnetic heating abilities by reducing Brownian motion. The results for internal energy change

calculations are based on theoretical MNP loading values and give a conservative $\frac{\Delta U}{m_{Fe_3O_4}}$

estimate for the magnetic micelles. This is an interesting observation that requires further

investigation to determine the effect of MNP concentration and confinement on magnetic

heating.

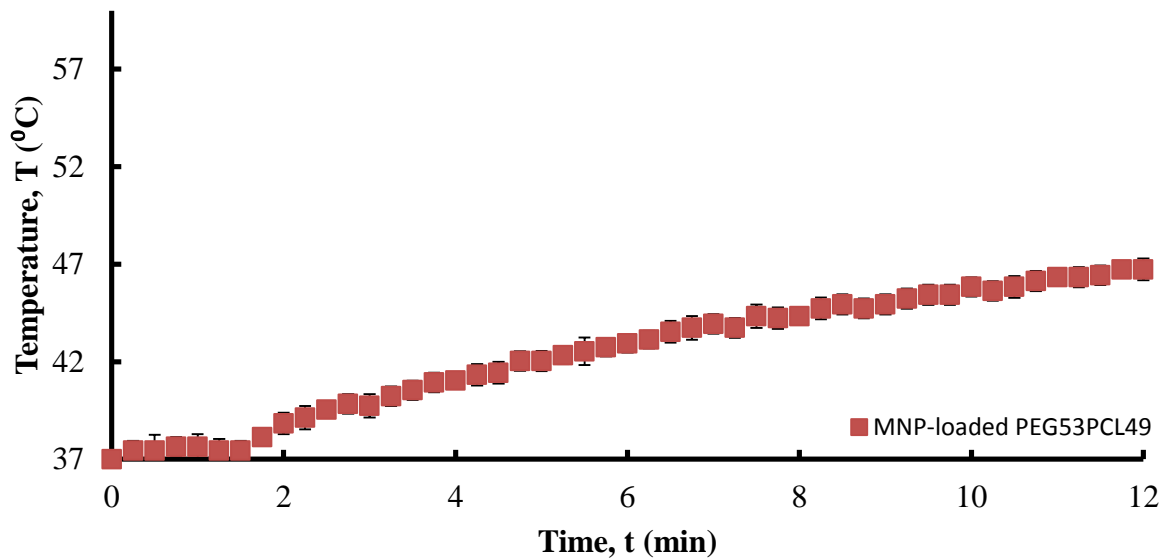


Figure 6.7. Magnetic heating curves for MNP-loaded PEG₅₃PCL₄₉ micelle sample in PBS pH 7.7 using 4-turn coil at a magnetic field strength of 82.7 kA/m and a frequency of 266 kHz. Error bars represent the standard deviation for n=3, in some cases error bars are smaller than the marker.

Table 6.2. Calculated added energy values for Fe₃O₄ MNPs in hexane and magnetic micelles in PBS pH 7.7 heated by an AC magnetic field with a fixed frequency of 266 kHz at three magnetic field strengths.

<i>H</i> (kA/m)	Fe ₃ O ₄ MNPs in hexane		Magnetic micelles	
	ΔT (K)	$\Delta U/m_{MNP}$ (J/g)	ΔT (K)	$\Delta U/m_{MNP}$ (J/g)
82.7	13.8	2480.0	0.29	14290
74.2	12.9	2310.0	0.25	12380
55.7	8.6	1540.0	0.11	5714

6.2 Drug release

Drug release experiments were performed on triamterene-loaded PEG₄₂PCL₁₉ micelles and Dox-loaded PEG₅₃PCL₄₉ micelles at 37 °C and 57 °C with external magnetic field pulses.

6.2.1 Triamterene release

Triamterene was loaded as a model drug into PEG₄₂PCL₁₉ micelles, which exhibited DLS size results with a narrow size distribution (number average size of 61+/- 1 nm) and were stable in solution for up to 4 weeks. The theoretical loading content of triamterene per polymer mass was 10% wt. Triamterene was observed in the dialysate immediately upon insertion into the 37 °C medium. This may have been due to incomplete separation of the micelles from free triamterene molecules. However, since the same sample of micelles was transferred from one temperature bath to another to monitor continued release, any acceleration in drug release at the elevated temperature is still significant. Upon heating to 47 °C, triamterene release accelerated for a short time. In Figure 6.5, an increase in slope can be seen after the rise in temperature at 20 minutes. This acceleration in drug delivery is more significant than it may appear in Figure 6.8. The concentrations measurements up to the 20 minute mark had a sequential additive effect on the next measurement since only 1 mL samples were taken at a time. However, at the 20 minute mark, the Float-A-Lyzer device was removed from its medium at 37 °C and placed in a fresh 100 mL dialysate with no free triamterene, still concentration measurements showed increasingly higher values than those leading up to the temperature switch. As the drug release duration approached 40 minutes, the released drug concentration calculated by UV-Vis actually begins to drop, likely due to experimental error. This preliminary study showed promise that thermo-responsive release from PEG-PCL micelles was possible.

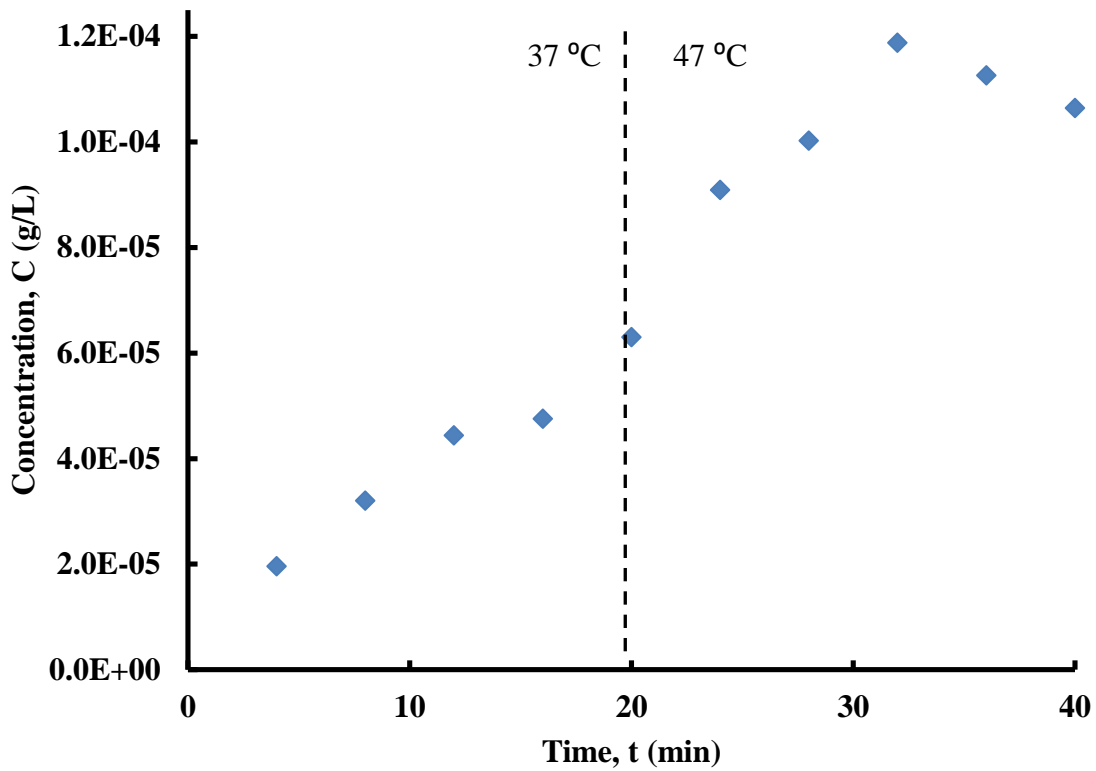


Figure 6.8. Release of triamterene from PEG₄₂PCL₁₉ micelles subjected to temperature increase from 37 °C to 47 °C after 20 minutes.

6.2.2 Temperature-dependent Dox release

Dox-loaded micelles were prepared from PEG₅₃PCL₄₉ diblock copolymers through a solvent evaporation method with a theoretical loading percentage of 26% wt polymer. After 4°C- dialysis during the preparation procedure doxorubicin was visible in the dialysate suggesting actual drug loading to be lower though this was not quantified. The Dox-loaded micelles were investigated for temperature-dependent drug release using water bath controlled temperatures. Doxorubicin release was seen early for both the 37 °C and 57 °C runs, however significantly accelerated release at 57 °C is seen within 1 hour (Figure 6.9). After 3 hours, drug release at 57 °C had released nearly doubled that released at 37 °C. By that point on average 2.91×10^{-5} grams of doxorubicin had been released at 57 °C while 1.66×10^{-5} grams had been released at 37 °C. Release began to level off at 6 hours at 57 °C, while similar slowing of doxorubicin release didn't occur until near the 24 hour mark. Operator error contributed to the larger error bars for the release at 37 °C experiments.

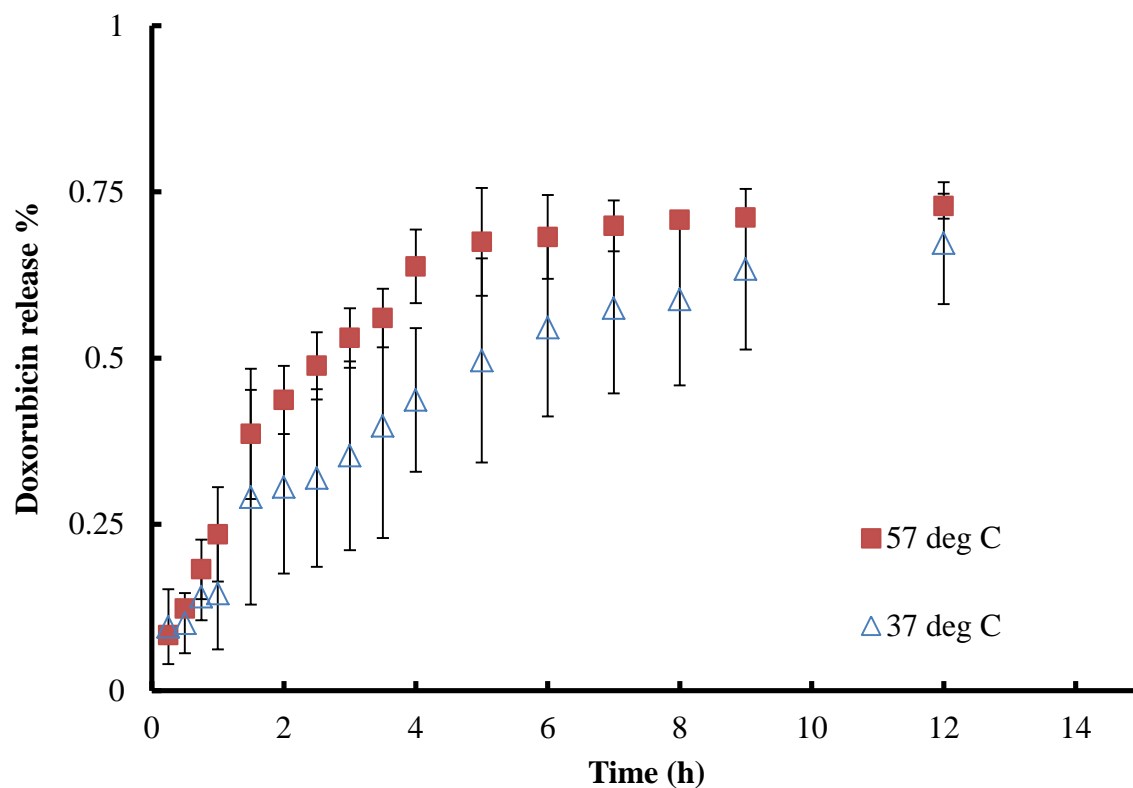


Figure 6.9. Doxorubicin release from PEG₅₃PCL₄₉ micelles at 37 °C and 57 °C based on theoretical loading of 19 wt%. Error bars represent standard deviation for replicate trials, n=3. In some cases error bars are smaller than the marker.

6.2.3 Magnetically-activated drug release investigation

Dox-loaded magnetic micelles were prepared to study an applied magnetic field's ability to trigger drug release. Extremely low and inconsistent absorbance measurements were obtained during the entirety of the planned experimental procedure which included two 30 min pulses with exposure to a 82.7 kA/m, 266 kHz magnetic field. These observations may be due to a slightly lowered loading percentage of doxorubicin, doxorubicin instability, or erratic behavior of the UV-Vis spectra of doxorubicin at low concentrations. Release was allowed to continue in a water bath at room temperature for up to 3 days, before different data collection method was performed. The experiment became an opportunity for method development Samples were extracted from the inside of the Float-A-Lyzer dialysis devices to see if any loss of absorbance when compared to the original Dox-loaded magnetic micelle solution absorbance. Figure 6.10 shows the comparison between samples from drug release with and without two 30 min magnetic field pulses. The steeper decrease in release trials exposed to magnetic field pulses indicates there was likely accelerated drug release, perhaps just not at a high enough rate to reach concentrations suitable for UV-Vis absorbance measurements. This study suggests a change to designing drug release experiments to allow for the measurement of the more concentrated solution within the dialysis device instead of the dilute dialysate release medium.

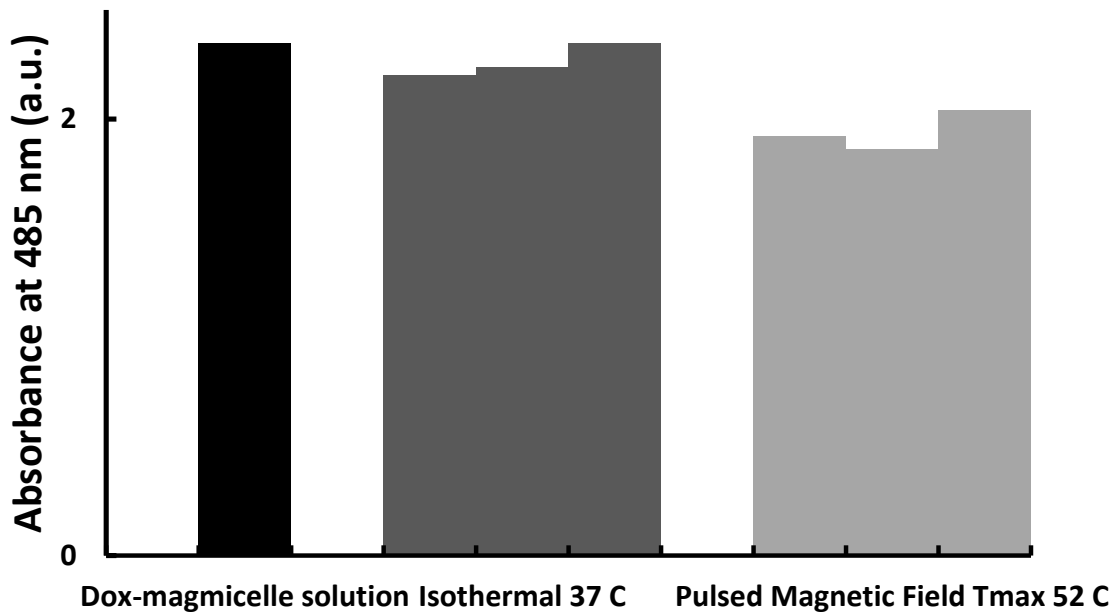


Figure 6.10. Absorbance values of triple replicate trials of drug release from Dox-loaded PEG₅₃PCL₄₉ micelles—either with pulsed exposure to a 82.7 kA/m, 266 kHz magnetic field, or at a constant 37 °C. The far left bar is the absorbance of the Dox-micelle solution prior to release. Remaining bars represent a single replicate trial with absorbance measurements taken either at the 64 hour time mark (left most of triple replicate bars for 37 °C and pulsed release), or at 48 hours (two replicate bars to the right for 37 °C and pulsed release)

Chapter 7

CONCLUSIONS

Fe_3O_4 nanoparticles were successfully synthesized through thermal decomposition and dispersed in hexane for magnetic induction heating investigations. Magnetic heating curves of these particles exposed to AC magnetic fields of various intensities and frequencies show magnetite particles are more than capable of reaching temperatures needed to achieve magnetically-activated release and/or hyperthermia effects. 4-turn and 6-turn solenoids were more likely to create magnetic fields suitable for magnetic hyperthermia therapy.

Magnetite SAR values increased as the magnetic field strength of an applied AC magnetic field increased. This agrees with the relationship given by the Rosensweig equation (2.3) [53]. The SAR values obtained for the custom synthesized magnetite particles are on the order typical of other reported iron oxide MNPs used for hyperthermia. [63-66]. Altering the frequency was also shown to have an effect on heating with increased SAR values for higher frequencies.

PEG-b-PCL diblock copolymers successfully self-assembled to trap magnetite nanoparticles into the core of magnetic micelles, as well as Dox-loaded magnetic micelles. Such formulations are able to heat to hyperthermic temperatures and showed an increase in internal energy added in magnetic heating experiments compared to Fe_3O_4 MNPs in hexane. Further studies are needed to evaluate the reasons why heating was more pronounced when the MNPs

were at a lower concentration and confined inside the micelles dispersed in PBS buffer solution as opposed to freely dispersed in hexane.

Drug release studies, showed triamterene- and doxorubicin- loaded micelles exhibited a temperature-dependent acceleration of drug release at temperatures above 42 °C, showing potential for magnetically triggered release. Difficulties detecting doxorubicin in aqueous solutions at very low concentrations hindered magnetically-activated drug release experiments. However, simple procedural, such as sampling from inside the dialysis device, may overcome similar problems in the future.

Chapter 8

RECOMMENDATIONS

While the experiments in this thesis were able to verify the potential of magnetite MNPs to heat for applications in hyperthermia and DDS, a few considerations may benefit future investigators to better understand the mechanisms of heating and

Implementing an already- purchased optical fluorescence decay probe (MicroMaterials, Inc., Tampa, FL) immune to interference from high magnetic fields into the experiment instrumentation for magnetic heating experiments could be a great asset. The device can upload temperature data to a computer four times per second, and can be placed directly inside MNP solutions. This could prove very important for SAR calculations that rely heavily on initial temperature changes. The probe may also give more accurate temperature data as it is submersible in sample solutions and will not measure only the temperature of the fluid surface as with an infrared camera. It should be noted the fluorescence decay probe comprised of a liquid crystal sensing tip is fragile. The infrared camera can still serve the purpose of monitoring induction coil surface temperature which may be responsible for some heating.

A careful study on drug and MNP loading in micelle preparation would be important to the overall project. Quantifying the amount of free drug or MNPs after micelle formulation is a challenge as many separation techniques on this scale leave the undesired product unreachable (as in syringe filters) or undetectable (as in 4 °C dialysis). Mastering lyophilization and atomic

absorption analysis techniques may be the key to better understanding the composition of our micelle formulations.

To prevent premature anti-cancer drug release from the micelles, the use of a biodegradable cross-linker may be considered to prolong drug entrapment. Cystamine has been used as a cross-linking agent to introduce disulfide bonds to micelle polymers in a drug delivery device [73]. The cross-links would be thermo-sensitive to maintain magnetic-triggering capabilities.

REFERENCES

- [1] Connel, P., and S. Hellman, "Advances in radiotherapy and implications for the next century: a historical perspective". *Cancer Research*, 69 (2) (2009) 383-92.
- [2] Gilman, A., "The initial clinical trial of nitrogen mustard". *American Journal of Surgery*. 105 (5) (1963) 574–578.
- [3] Takimoto, C., and E. Calvo "Principles of Oncologic Pharmacotherapy." in Pazdur R, Wagman, L., Camphausen, K., and W. Hoskins (Eds) 11th ed. *Cancer Management: A Multidisciplinary Approach*. San Francisco, CA: CMP Healthcare Media LLC, 2008.
- [4] van der Zee, J., "Heating the patient: a promising approach?" *Annals of Oncology*, 13(8) (2002) 1173–1184.
- [5] Jones, E., Oleson, J. and E. Posnitz., "A randomized trial of hyperthermia and radiation for superficial tumors." *Journal of Clinical Oncology*, 23(13) (2005) 3079-3085.
- [6] Wust, P., Hildebrandt B, Sreenivasa G, and B. Rau, "Hyperthermia in combined treatment of cancer." *Lancet Oncology*, 2 (2002) 487-497.
- [7] Bicher, H., Hetzel, F., Sandhu, T., Frinak, S., Vaupel, P., O'Hara, M., and T. O'Brien, "Effects of hyperthermia on normal and tumor microenvironment." *Radiology*, 137 (1980) 523-530.
- [8] Hehr, T., Wust, P., Bamberg, M., and W. Budach, "Current and potential role of thermoradiotherapy for solid tumours." *Oncologie*, 26 (2003) 295-302.
- [9] Braun, J., and Hahn, G. M. "Enhanced cell killing by bleomycin and 43°C hyperthermia and the inhibition of recovery from potentially lethal damage." *Cancer Research*, 35: 2921 -2927, 1975.
- [10] Dahl O, Dalene R, Schem BC, Mella O. "Status of clinical hyperthermia. *Acta Oncology*, 38 (7) (1999) 863-73.
- [11] Falk, M., and R. Issels, "Hyperthermia in oncology." *International Journal of Hyperthermia*, 17 (1) (2001) 1-18.
- [12] Choy, H., and D. Kim, "Chemotherapy and irradiation interaction". *Seminars in Oncology*, 30 (2003) 3–10.

- [13] Issels, R., Lindner, L., Verweij, J., Wust, P., Reichard, P., Schem, B., Abdel-Rahman, S., Daugaard, S., Salat, C., Wendtner, C., Vujaskovic, Z., Wessalowski, R., Jauch, K., Durr, H., Ploner, F., Baur-Melnyk, A., Mansmann, U., Hiddemann, W., Blay, J., and P. Hohenberger, P., “Neo-adjuvant chemotherapy alone or with regional hyperthermia for localized high-risk soft-tissue sarcoma: a randomized phase 3 multicentre study.” *The Lancet Oncology*, 11 (6) (2010) 561-570.
- [14] Westermann, A., Jones, E., Baard-Christian, S., van der Seen-Banasik, E., Koper, P., Mella, O., Uitterhoeve, A., Witt, R., van der Velden, J., Burger, C., vander Wilt, C., Dahl, O., Prosnitz, L., and J. van der Zee, “First results of triple-modality treatment combining radiotherapy, chemotherapy, and hyperthermia for the treatment of patients with stage IIB, III, and IVA cervical carcinoma.” *Cancer*, 104 (4) (2005) 763-770.
- [15] Kost, J., and R. Langer, “Responsive polymeric delivery systems,” *Advanced Drug Delivery Reviews*, 46 (2001) 125-148.
- [16] Lohmann, D., “Controlled release – recent progress in polymeric drug delivery systems” *Macromolecular Symposia*, 100 (1) (1995) 25-30.
- [17] Liechty, W., Kryscio, D., Slaughter, B., and N. Peppas, “Polymers for drug delivery systems.” *Annual Review of Chemical and Biomolecular Engineering*, 1 (2010) 149-173.
- [18] Kim, S., Kim, J., Jeon, O., Kwon, I., and K Park, “Engineered polymers for advanced drug delivery.” *European Journal of Pharmaceutics and Biopharmaceutics*, 71 (2009) 420-430.
- [19] Husseini, G., El-Fayoumi, R., O’Neil, K., Rappaport, N., and W. Pitt, “DNA damage induced by micellar-delivered doxorubicin and ultrasound: comet assay study.” *Cancer Letters*, 154 (2000) 211-216.
- [20] Kim, S., Kim, J., Jeon, O., Kwon, I., Park, K., “Engineered polymers for advanced drug delivery” *European Journal of Pharmaceutics and Biopharmaceutics*, 71 (2009) 420-430.
- [21] Lee, E., Na, K. and Y. Bae, “Doxorubicin loaded pH-sensitive polymeric micelles for reversal of resistant MCF-7 tumor.” *Journal of Controlled Release*, **103** (2005) 405–418.
- [22] Gref, R., Minamitake, Y., Peracchia, M., Trubetskoy, V., Torchilin, V and R. Langer, “Biodegradable long-circulating polymeric nanospheres.” *Science*, **263** (1994) 1600–1603.
- [23] Harper, G., Davies, M., Davis, S., Tadros, T., Taylor, D., Irving, M., and J. Waters, “Steric stabilization of microspheres with grafted polyethylene oxide reduces phagocytosis by rat Kupffer cells in vitro.” *Biomaterials*, 12 (1991) 695–700.
- [24] Cirstoiu-Hapca, A., Bossy-Nobs, L., Buchegger, F., Gurny, R., and F. Delie, “Differential tumor cell targeting of anti-HER2 (Herceptin) and anti-CD20 (Mabthera) coupled nanoparticles.” *International Journal of Pharmacy*, 331 (2007) 190–196.

- [25] Wang, S., and P. Low, "Folate-mediated targeting of antineoplastic drugs, imaging agents and nucleic acids to cancer cells." *Journal of Controlled Release*, 53 (1-3) (1998) 39-48.
- [26] Chen, K., and X. Chen, "Integrin targeted delivery of chemotherapeutics." *Theranostics*, 1 (2011) 189-200.
- [27] Li, P., Liu, Y., Maynard, J., Tang, Y., and A. Deisseroth, "Use of adenoviral vectors to target chemotherapy to tumor vascular endothelial cells suppresses growth of breast cancer and melanoma." *Molecular Therapy*, 18 (5) (2010) 921-928.
- [28] Guan, H., McGuire, M., Li, S., and K. Brown, "Peptide-targeted polyglutamic acid doxorubicin conjugates for the treatment of $\alpha\beta6$ -positive cancers." *Bioconjugate Chemistry*, 19(9) (2008) 1813-21.
- [29] O'Neal, D., Hirsch, L., Halas, N., Payne, J., and J. West, "Photo-thermal tumor ablation in mice using near infrared-absorbing nanoparticles." *Cancer Letters*, 209 (2) (2004) 171-176.
- [30] Ruehm, S., Corot, C., Vogt, P., Kolb, S., and J. Debatin, "Magnetic resonance imaging of atherosclerotic plaque with ultrasmall superparamagnetic particles of iron oxide in hyperlipidemic rabbits." *Circulation*, 103 (3) (2001) 415-422.
- [31] Weissleder, R., Elizondo, G., Wittenberg, J., Rabito, C., Bengel, H., L. Josephson, "Ultrasmall Superparamagnetic Iron-Oxide - Characterization of a New Class of Contrast Agents for Mr Imaging." *Radiology*, 175 (2) (1990) 489-493.
- [32] Brannon-Peppas, L., and J. Blanchette, "Nanoparticle and targeted systems for cancer therapy." *Advanced Drug Delivery Reviews*, 61 (4) (2009) 364-364.
- [33] Satarkar, N., and J. Hilt, "Magnetic hydrogel nanocomposites for remote controlled pulsatile drug release." *Journal of Controlled Release*, 130 (3) (2008) 246-251.
- [34] Yu, C., Al-Saadi, A., Shih, S., Qiu, L., Tam, K., and S. Tsang, "Immobilization of BSA on Silica-Coated Magnetic Iron Oxide Nanoparticle." *Journal of Physical Chemistry, C*, 113 (2) (2009) 537-543.
- [35] Chen, F., Zhang, L., Chen, Q., Zhang, Y., and Z. Zhang, "Synthesis of a novel magnetic drug delivery system composed of doxorubicin-conjugated Fe_3O_4 nanoparticle cores and a PEG-functionalized porous silica shell." *Chemical Communications*, 46 (45) (2010) 8633-8635.
- [36] Kim, T., Kim, J., Shim, W., Kim, S., Park, T., Jung, J., "Tracking of transplanted mesenchymal stem cells labeled with fluorescent magnetic nanoparticle in liver cirrhosis rat model with 3-T MRI." *Magnetic Resonance Imaging*, 28 (7) (2010) 1004-1013.
- [37] Sun, C., Lee, J., and M. Zhang, "Magnetic nanoparticles in MR imaging and drug delivery." *Advanced Drug Delivery Reviews*, 60 (11) (2008) 1252-1265.

- [38] Gupta, A., and M. Gupta, "Synthesis and surface engineering of iron oxide nanoparticles for biomedical applications." *Biomaterials*, 26 (18) (2005) 3995-4021.
- [39] Gupta, A., Naregalkar, R., Vaidya, V., and M. Gupta, "Recent advances on surface engineering of magnetic iron oxide nanoparticles and their biomedical applications." *Nanomedicine-Uk*, 2 (1) (2007) 23-39.
- [40] Lu, A., Salabas, E., and F. Schuth, "Magnetic nanoparticles: Synthesis, protection, functionalization, and application." *Angewandte Chemie International Edition* 46 (8) (2007) 1222-1244.
- [41] Hao, R., Xing, R., Xu, Z., Hou, Y., Gao, S., and S. Sun, "Synthesis, functionalization, and biomedical applications of multifunctional magnetic nanoparticles." *Advanced Materials*, 22 (25) (2010) 2729-2742.
- [42] Laurent, S., Forge, D., Port, M., Roch, A., Robic, C., Elst, L., and R. Muller, "Magnetic iron oxide nanoparticles: Synthesis, stabilization, vectorization, physicochemical characterizations, and biological applications." *Chemical Reviews* 108 (6) (2008) 2064-2110.
- [43] Sun, S., Hao, Z., Robinson, D., Raoux, S., Rice, P., Wang, S., and G. Li, "Monodisperse MFe_2O_4 (M = Fe, Co, Mn) nanoparticles." *Journal of the American Chemical Society*, 126 (1) (2004) 273-279.
- [44] Herve, K., Douziech-Eyrolles, L., Munnier, E., Cohen-Jonathan, S., Souce, M., Marchais, H., Limelette, P., Warmont, F., Saboungi, M., Dubois, P., and I. Chourpa., "The development of stable aqueous suspensions of PEGylated SPIONs for biomedical applications." *Nanotechnology*, 19 (46) (2008) 465608.
- [45] Park, J., Daksha, P., Lee, G., Woo, S., and Y. Chang, "Highly water-dispersible PEG surface modified ultra small superparamagnetic iron oxide nanoparticles useful for target-specific biomedical applications." *Nanotechnology* **2008**, 19 (36), 365603.
- [46] Mornet, S., Portier, J., and E. Duguet, "A method for synthesis and functionalization of ultrasmall superparamagnetic covalent carriers based on maghemite and dextran." *Journal of Magnetism and Magnetic Materials*, 293 (1) (2005) 127-134.
- [47] Donadel, K., Felisberto, M., Favere, V., Rigoni, M., Batistela, N., and M. Laranjeira, "Synthesis and characterization of the iron oxide magnetic particles coated with chitosan biopolymer." *Materials Science and Engineering C -Bio S*, 28 (4) (2008) 509-514.
- [48] Ho, K., and P. Li, "Design and synthesis of novel magnetic core-shell polymeric particles." *Langmuir*, 24 (5) (2008) 1801-1807.
- [49] Kim, E., Ahn, Y., and H. Lee, "Biomedical applications of superparamagnetic iron oxide nanoparticles encapsulated within chitosan." *Journal of Alloys and Compounds* 434 (2007) 633-636.

- [50] Hagspiel, K., Neidl, k., Eichenberger, A., Weder, W., and B. Marincek, “Detection of liver metastases—comparison of superparamagnetic iron oxide-enhanced and unenhanced MR-imaging at 1.5 T with dynamic CT, intraoperative US, and percutaneous US.” *Radiology*, 196 (1995) 471–478.
- [51] Blakeborough, A., Ward, J., Wilson, D., Kajiya, Y., Guthrie, A., and P. Robinson, “Superparamagnetic iron oxide improves the detection of liver lesions at MR imaging: multiobserver study with AFROC analysis.” *Radiology* 201 (1996) 1038.
- [52] Duguet, E., Vasseur, S., Mornet, S., Goglio, G., Demourgues, A., Portier, J., Grasset, F., Ververka, P., and E. Pollert, “Towards a versatile platform based on magnetic nanoparticles for in vivo applications,” *Bulletin of Materials Science*, 29 (2006) 581-586.
- [53] Rosensweig, R., “Heating magnetic fluid with alternating magnetic field.” *Journal of Magnetism and Magnetic Materials*, 252 (1-3) (2002) 370-374.
- [54] Arkin, H., Xu, L., and K. Holmes, “Recent developments in modeling heat transfer in blood perfused tissues.” *IEEE Transactions on Biomedical Engineering*, 41 (1994) 97–107.
- [55] Gupta, P., Jitendra, S., and K. Rai, “Numerical simulation for heat transfer in tissues during thermal therapy.” *Journal of Thermal Biology*, 35 (6) (2010) 295-301.
- [56] Laurent, S., Dutz, S., Hafeli, U., and M. Mahmoudi, “Magnetic fluid hyperthermia: Focus on superparamagnetic iron oxide nanoparticles.” *Advances in Colloid and Interface Science*, 166 (1-2) (2011) 8-23.
- [57] Brezovich, I., “Low frequency hyperthermia: capacitive and ferromagnetic thermoseed methods.” *Medical Physics Monograph Medical Physics*, 16 (1988) 82.
- [58] Jordan, A., “MagForce® Nanotherapy: with tumor-specific nanoparticles against cancer.” *VDI Berichte* (2005) 111–116.
- [59] Jordan, A., and K. Maier-Hauff, “Magnetic nanoparticles for intracranial thermotherapy.” *Journal of Nanoscience and Nanotechnology*, 7 (12) (2007) 604–4606.
- [60] Jordan, A., Scholz, R., Maier-Hauff, K., van Landeghem, F., Waldoefner, N., and U. Teichgraeber, *et al.* “The effect of thermotherapy using magnetic nanoparticles on rat malignant glioma.” *Journal of Neurological Oncology*, **78** (1) (2006), 7–14.
- [61] Thiesen, B., and A. Jordan, “Clinical applications of magnetic nanoparticles for hyperthermia.” *International Journal of Hyperthermia*, **24** (6) (2008), 467–474.
- [62] Zhang, L., Gu, H., and X. Wang, “Magnetite ferrofluid with high specific absorption rate for application in hyperthermia.” *Journal of Magnetism and Magnetic Materials*, 311 (2007) 228-233.

- [63] Ma, M., Wu, Y., Zhou, J., Sun, Y., Zhang, Y., and N. Gu, "Size dependence of specific power absorption of Fe₃O₄ particles in AC magnetic field." *Journal of Magnetism and Magnetic Materials*, 268 (1-2) (2004) 33-39.
- [64] Baker, I., Zeng, Q., Li, W., and C. Sullivan, "Heat deposition in iron oxide and iron nanoparticles for localized hyperthermia." *Journal of Applied Physics*, 99 (2006) 08H106.
- [65] Muller, R., Hergt, R., Zeisberger, M., Gawalek, W., "Preparation of magnetic nanoparticles with large specific loss power for heating applications." *Journal of Magnetism and Magnetic Materials*, 289 (2005) 13-16.
- [66] Jordan, A., Scholz, R., Wust, P., Schirra, H., Thomas, S., Schmidt, H., and R. Felix, "Endocytosis of dextran and silan-coated magnetite nanoparticles and the effect of intracellular hyperthermia on human mammary carcinoma cells in vitro." *Journal of Magnetism and Magnetic Materials*, 194 (1999) 185-196.
- [67] Satarkar, N., and J. Hilt, "Magnetic hydrogel nanocomposites for remote controlled pulsatile drug release." *Journal of Controlled Release*, 130 (3) (2008) 246-251.
- [68] Herrera, A., Rodriguez, M., Torres-Lugo, M., and C. Rinaldi, "Multifunctional magnetite nanoparticles coated with fluorescent thermo-responsive polymeric shells." *Journal of Materials Chemistry*, 18 (8) (2008) 855-858.
- [69] Sanson, C., Diou, O., Thevenot, J., Ibarbourne, E., Soum, A., Brulet, A., Miraux, S., Thiaudiere, E., Tan, S., Brisson, A., Dupuis, V., Sandre, O. and Lecommandoux, S., "Doxorubicin loaded magnetic polymersomes: Theranostic Nanocarriers for MR Imaging and Magneto-Chemotherapy." *ACS Nano*, 5 (2) (2011) 1122-1140.
- [70] Nikles, S., Nikles, J., Hudson, J., and D. Nikles, "Diblock copolymers for magnetically triggered drug delivery systems." *Journal of Science and Health at the University of Alabama*, 7 (2010) 35-39.
- [71] Lide, D., ed. *CRC Handbook of Chemistry and Physics*, 88th edition, Taylor & Francis Group Boca Raton, Florida, (2008).
- [72] Crescenzi, V., Manzini, G., Calzolari, G., and C. Borri, "Thermodynamics of fusion of poly-β-propiolactone and poly-ε-caprolactone. comparative analysis of the melting of aliphatic polylactone and polyester chains." *European Polymer Journal*, 8 (3) (1972) 449-463.
- [73] Kim, J., Sahay, G., Kabanov, A., and T. Bronich, "Polymeric micelles with ionic cores containing biodegradable cross-links for delivery of chemotherapeutic agents." *Biomacromolecules*, 11 (4) (2010) 919-926.

APPENDIX

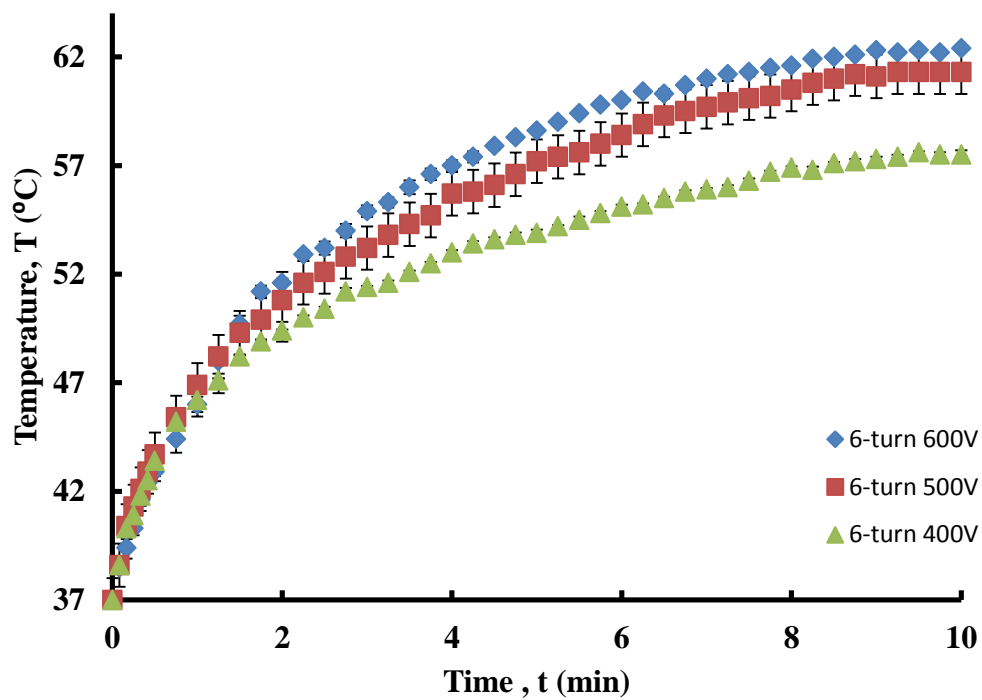


Figure A1.1 Heating curves for 8.4 g/L Fe_3O_4 in hexane using a 6-turn coil at voltage setting of 400, 500, and 600V at a frequency of 265 kHz. Error bars represent standard deviation for replicate trials, $n=3$. In some cases error bars are smaller than the marker.

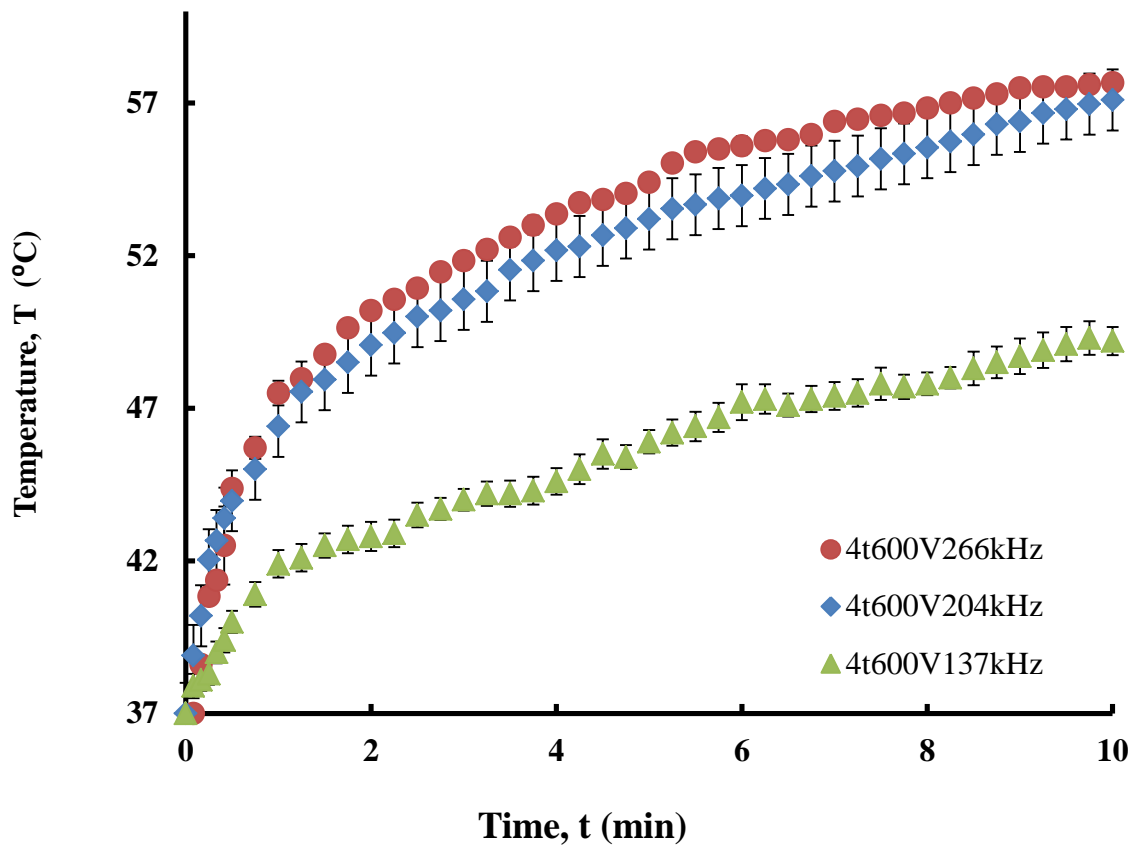


Figure A1.2 Magnetic heating curves for 8.4 g/L Fe_3O_4 in hexane using a 4-turn coil at a voltage setting of 600V at frequencies of 266, 204, and 137 kHz. Error bars represent standard deviation for replicate trials, $n=3$. In some cases error bars are smaller than the marker.

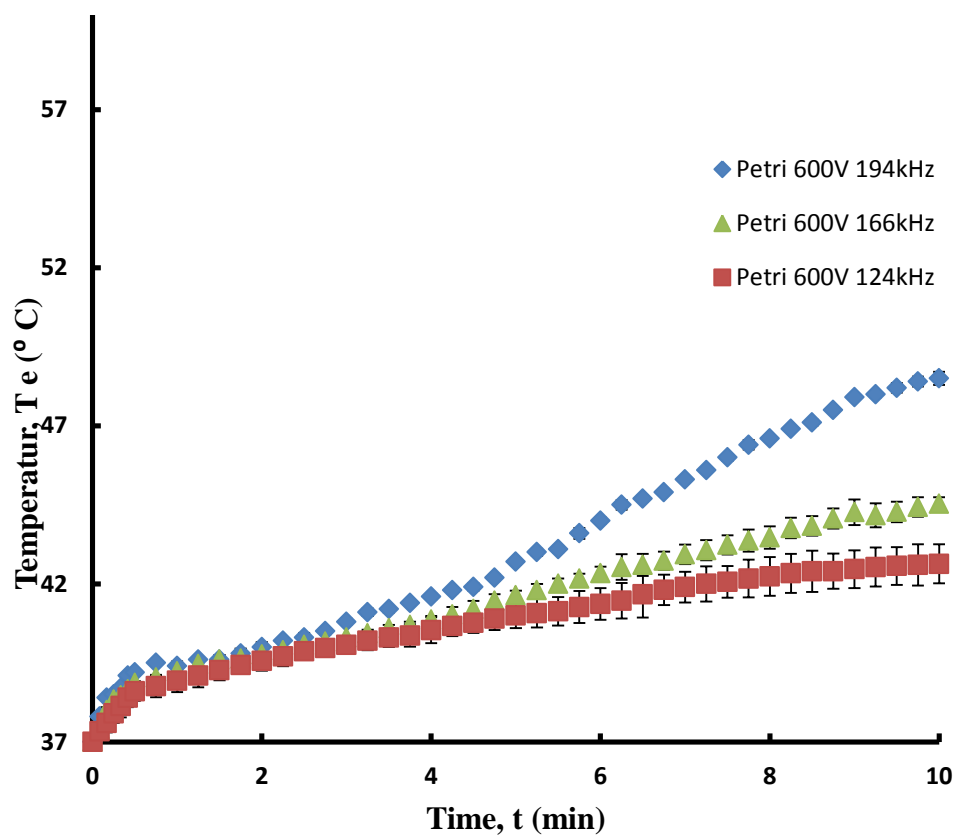


Figure A1.3 Magnetic heating curves for 8.4 g/L Fe_3O_4 in hexane using a Petri dish coil at a voltage setting of 600V at frequencies of 194, 166, and 124 kHz. Error bars represent standard deviation for replicate trials, $n=3$. In some cases error bars are smaller than the marker.

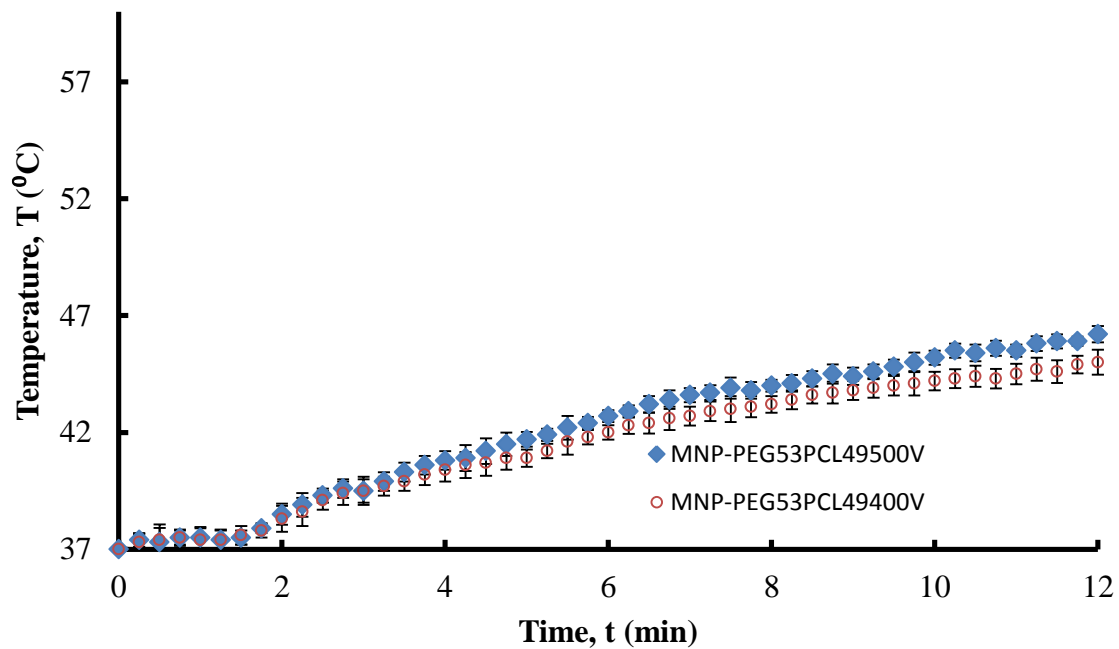


Figure A1.4 Magnetic heating curves for magnetic micelles. Fe_3O_4 -loaded $\text{PEG}_{53}\text{PCL}_{49}$ micelles in PBS pH 7.7 were heated using a 4-turn coil at voltage settings of 400 and 500 V and a frequency of 266 kHz. Error bars represent standard deviation for replicate trials, $n=3$. In some cases error bars are smaller than the marker.

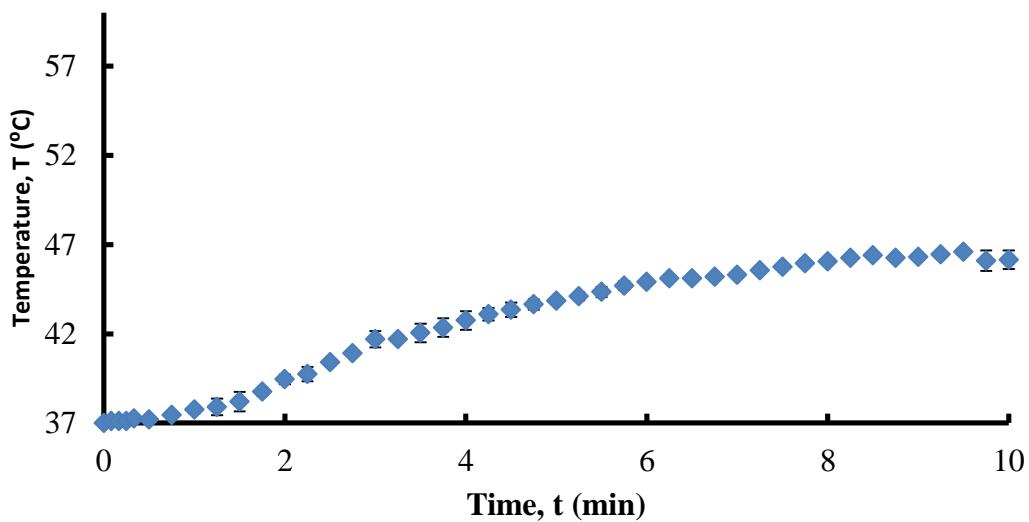


Figure A1.5 Magnetic heating curves for 98% pure hexane using a 6-turn coil. 0.5 mL hexane was heated at a voltage of 600 V and a frequency of 265 kHz. Error bars represent standard deviation for replicate trials, $n=3$. In some cases error bars are smaller than the marker.

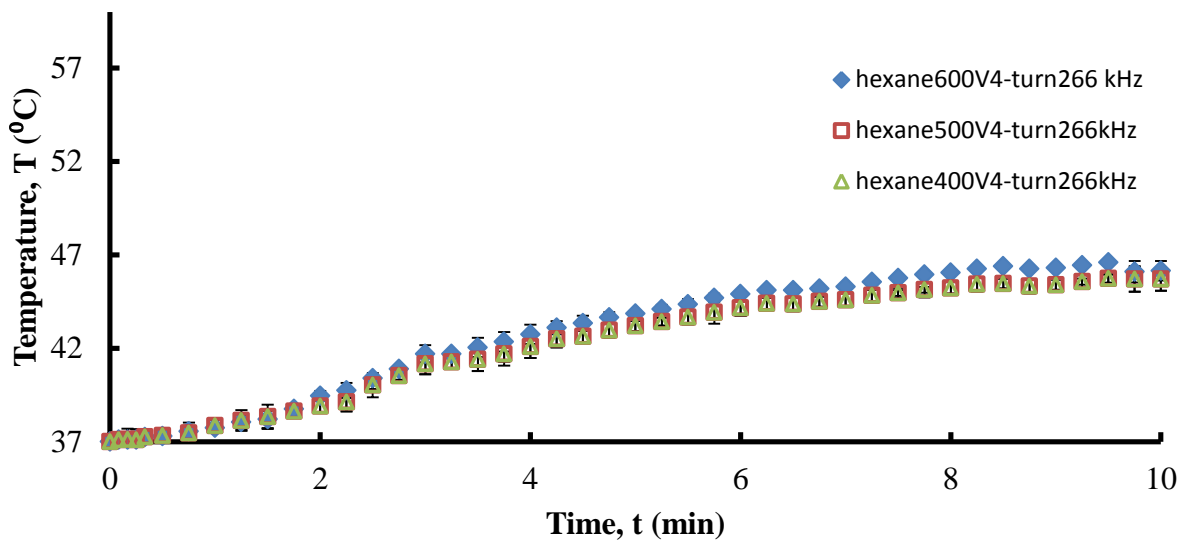


Figure A1.6 Magnetic heating curves for 98% pure hexane using a 4-turn coil. 0.5 mL hexane was heated voltage settings of 600, 500, and 400 V and a frequency of 266 kHz. Error bars represent standard deviation for replicate trials, n=3. In some cases error bars are smaller than the marker.

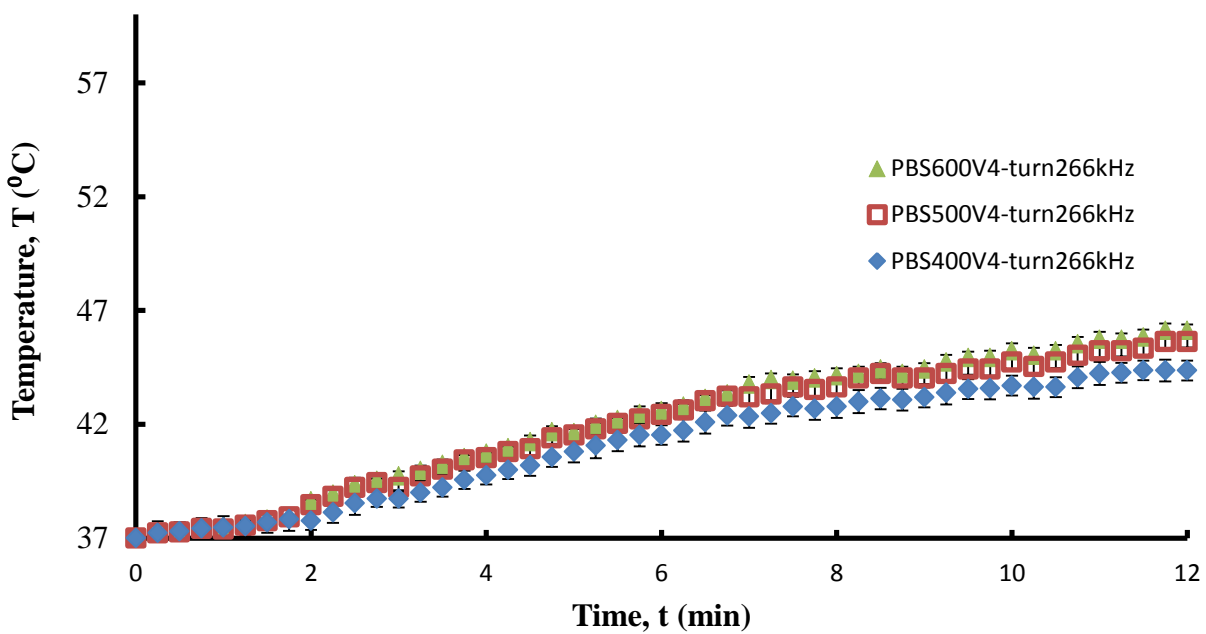


Figure A1.7 Magnetic heating curves for PBS pH 7.7. PBS (0.5 mL) was heated using a 4-turn coil at voltage settings of 600, 500, and 400V and a frequency of 266 kHz. Error bars represent standard deviation for replicate trials, n=3. In some cases error bars are smaller than the marker.